



Ion-partitioning effects on electrokinetic flow of generalized Maxwell fluids through polyelectrolyte layer-coated nanopore under AC electric field

Priyanka Koner¹ · Subrata Bera¹ · Hiroyuki Ohshima²

Received: 20 April 2021 / Revised: 10 August 2021 / Accepted: 12 August 2021 / Published online: 29 September 2021
© The Author(s), under exclusive licence to Springer-Verlag GmbH Germany, part of Springer Nature 2021

Abstract

The article dealt with an analytic study on the electroosmotic flow and mass transport of an electro neutral solute through polyelectrolyte layer (PEL)-coated canonical nanopore under the imposed alternative current electric field for Maxwell fluids. The PEL of uniform thickness contains positive charge density, while surface potential of nanopore is negatively charged. The permittivities of the electrolyte solution and PEL are assumed to be different which creates the ion-partitioning effects. The Born formula is incorporated to account the ion-partitioning effects. For low surface charge, the distribution of the ionic species are governed by the modified Boltzmann distribution and using the Debye–Hückel approximation, linearized Poisson–Boltzmann equation gives the distribution of induce potential inside and outside of the PEL. The modified Cauchy momentum equation with the Maxwell constitutive equation is used for the fluid flow distribution interior and exterior of the PEL. The analytic solutions for the distribution of induced potential and axial velocity are established using modified Bessel function for the Maxwell fluid. The importance of the bulk ionic concentration, oscillating Reynolds number, PEL fixed charge density, relaxation time, permittivity ratio between PEL and electrolyte solution and softness parameter is studied in this investigation. The convection–diffusion equation is considered to transport of neutral solute between two reservoirs, connected with nanopore. An analytic solution for the distribution of solute concentration is also presented. The effects of the flow characteristics on volumetric flow rate, average mass transport, and neutralization factor are described in this study.

Keywords Ion-partitioning effect · Maxwell fluids · Solute transport · Modified Cauchy momentum equation · Oscillating Reynolds number

Introduction

Micro- and nanofluidic devices have attracted considerable attention due to its versatile application like drug diagnostic [1, 2], separation of bio-macromolecules [3–5], DNA sequencing [6], and desalination of seawater [7] and environmental monitoring sensors [8] to name a few. These devices became growing more importance microelectromechanical system (MEMS), Lab-on-a-chip, etc., and it is designed as microchannels, micromixers, micropumps, nanopore, and

microreaction chambers. When electrolyte solution comes in contact with charged nanopore wall, electric double layer (EDL) forms at the wall surface due to the redistribution of counter-ions and co-ions in the electrolyte medium. Many important features were experimentally observed in nanofluidic devices when characteristic height is comparable to the EDL thickness. Electroosmotic flow (EOF) is the bulk liquid motion under the application of external electric field [9]. These devices use the electrokinetic effects such as electroosmosis to transport electro-neutral solute through the soft polyelectrolyte-coated nanopore. When wall surface of the nanopore is covered with soft polymeric material named as soft nanopore where the polyelectrolyte layer (PEL) is sandwiched between the rigid nanopore wall and bulk electrolyte medium. Due to several advantages of EOF such as plug-like velocity profile, negligible axial dispersion and better flow control, many research group studied in different aspect of EOF under the applied electric field.

✉ Subrata Bera
subrata@math.nits.ac.in

¹ Department of Mathematics, National Institute of Technology Silchar, Silchar, Assam 788010, India

² Faculty of Pharmaceutical Sciences, Tokyo University of Science, 2641 Yamazaki Noda, Chiba, Japan

A large volume of experimental, theoretical, and computational studies conducted for steady EOF and solute transport and mixing phenomena on the Newtonian fluid for different geometrical shape such as rectangular microchannel [10], cylindrical capillary [11], semi-circular microchannel [12], annulus [13], T-shape of microchannel [14], and surface-modulated microchannel [15] with heterogeneous surface potential. Relatively large DC electric field strength is required for such type of steady-state EOF which might not be always undesirable in many practical situation. By applying DC electric field in a microfluidic system, sometimes it may form gas bubbles. This may block the flow passage which may be suppressed under AC electric field. As a result, time-dependent EOF has become major growing attraction as an alternative mechanism for micro-fluidics transport. Dutta and Beskok [16] studied the time periodic EOF in two-dimensional rectangular microchannel and established the analytic solution for flow field under AC electric field. The control of time periodic flow rate under the pulsating electric fields through a circular microchannel has been studied by Chakraborty and Ray [17]. Jian et al. [18] analyzed the time periodic EOF through a cylindrical microannulus considering different zeta potentials in inner and outer cylinder using linear Poisson–Boltzmann equation for induced potential and Navier–Stokes equation for flow field. Huang and Lai [19] studied theoretically the enhancement of mass transport and species separation phenomena under an oscillatory EOF in a microchannel.

Polyelectrolyte-coated nanopore, nanometer size pore, or polyelectrolyte layer has motivated a great attraction among many research community for regulating ion transport and sensing single bio-polymers phenomena. EOF through a PEL-grafted nanochannel under the AC electric field has been investigated by Li et al. [20] using Debye–Hückel approximation. A theoretical studies on the ion transport phenomena through a poly electrolyte modified nanopore have been performed by Yeh et al. [21] using a continuum-based model. An analytic solution for transient EOF through the polyelectrolyte grafted nanochannel is derived by Li et al. [22] using Debye–Hückel approximation for Jeffrey fluid under the AC electric field. Chen and Das [23] investigated the electroosmotic transport through the pH-regulated polyelectrolyte-grafted nanochannel. Previously, it is considered that for low charging density in polyelectrolyte grafting which allows equal permittivity ratio between the electrolyte solution and PEL. Generally, the permittivity in the polyelectrolyte molecules is substantially less than the surrounding electrolyte solution, and hence depending on the PEL charge density, a significant impact occurs on the functional permittivity inside the PEL which creates the ion-partitioning effect. Physically, the Born energy [24], which transform the energy of an ion from bulk electrolyte solution to the PEL, determines the ion-partitioning effect. Poddar

et al. [25] studied the Born energy effects on pressure gradient induced electrokinetic flow through a soft charged layer in narrow fluidic conduit. Ganjizade et al. [26] studied the ion-partitioning effect in a spherical soft particle in the presence of volumetric core charge density. Reshadi and Saidi [27] analyzed theoretically the electro-hydrodynamics characteristic on combined electroosmotic and pressure-driven flow through polyelectrolyte-grafted nanotube considering steric effects. Maurya et al. [28] theoretically investigate the ion-partitioning effects on electrophoresis of a soft particle made up of a charged hydrophobic inner core surrounded with PEL.

Although most of authors studied the EOF for the Newtonian fluids but saliva solution, blood sample, DNA sample which are used to analyse in BioMENS devices, cannot be treated as Newtonian fluids. Many microfluidic devices are also uses non-Newtonian bio-fluids to analyse the physiology and medical applicant. The Cauchy momentum equation with a proper constitutive law are used to describe the fluid characteristics of these kind of fluids instead of the Navier–Stokes equation. Peralta et al. [29] studied theoretically the mass transport rate of an electro-neutral solute in EOF under the applied periodic electric field through an annular micro-annular region between two concentric cylinders with asymmetric and symmetric zeta potentials for Maxwell fluids. Analytic solutions for transient EOF velocity between parallel plate micro channel and micro tube for Maxwell fluids have been derived by Li et al. [30]. Using the Debye–Hückel approximation in electric potential, Liu et al. [31] derived an analytic solution of the magneto-hydrodynamical EOF velocity between two parallel plates for Maxwell fluid.

The aim of the study is to investigate theoretically the ion-partitioning effects on electroosmotic flow and solute transport phenomena of Maxwell fluid through the PEL-coated conical nanopore under the influence of the imposed AC electric field. The medium near the polyelectrolytes medium attached with electrolyte molecules of an aqueous solution. Being different permittivity between two medium, ion-partitioning effect occurs which is determined by the Born formula. With considering the ion-partitioning effects, the linearized Poisson Boltzmann equation gives the distribution of the induced potential and the Cauchy momentum equation with Maxwell constitute equation provide the distribution of the flow pattern in the exterior and interior of the PEL. The analytic expression for the solutions for the distribution of the induced electric potential and axial fluid velocity are established in this study. The convection–diffusion equation is also solved analytically to study the transport behaviour of electro neutral solute. The comparison between the Newtonian and Maxwell fluids are also addressed in this study. The main objective in this paper is to analyse the influence of oscillating Reynolds number, the permittivity ratio between

two layers, relaxation time, PEL fixed charge density, ionic concentration, softness parameter on electrokinetic flow and solute transport phenomena in Maxwell fluid.

Mathematical model

We have studied the unsteady EOF of a generalized Maxwell fluids under the influence of an external applied AC electric field through PEL grafted nanopore of radius a (Fig. 1). The nanopore is filled with an aqueous binary symmetric electrolyte of valence z_i ($i = 1, 2$) of density ρ . The dielectric constant of the PEL and electrolyte medium are considered to be different and denoted as ϵ_p and ϵ_e respectively when ϵ_0 is the vacuum permittivity. A PEL of uniform thickness d is embedded in the wall surface of the nanopore which is bearing uniform negative surface potential ζ^* . The PEL contains uniform volume charge density ρ_{fix} which stem from ionization of PEL molecule where $\rho_{fix} = ZFN$, where F is the Faraday constant, Z is the valence and N is the molar concentration of the PEL ions. The EDL is formed at the interfaces between the electrolyte solution and the inner surface of the cylinder and EDL thickness (λ_D) is the reciprocal of the Debye layer thickness $\kappa(= 1/\lambda_D = \sqrt{\sum_i(z_i e)^2 n_0 / \epsilon_0 \epsilon_e k_B T})$. Here, k_B is Boltzmann constant, T is absolute temperature, e is the elementary charge and n_0 is the bulk ionic concentration. When the permittivity of the polyelectrolyte ions is significantly less than that of the surrounding electrolyte medium, a substantial impact occurs on the effective permittivity inside the PEL, depending upon the grafting charge density [32]. Due to different dielectric permittivity of the PEL and electrolyte medium, a partition effects of ions ΔW_i [33] occur due to the change in self energy between these ions. The difference ionic concentration n_i of the i th species between the two medium can be related through the

ion-partitioning coefficient f_i as $n_i|_{r=a-d^-} = f_i n_i|_{r=a-d^+}$ [26, 32] The ion partition coefficient factor can be expressed as

$$f_i = \exp(-\Delta W_i / k_B T) \tag{1}$$

The Born energy ΔW_i determines the associated electrostatic free energy required to transfer an ion from the bulk solvent to the bulk of the PEL membrane, and it can be expressed as [33]

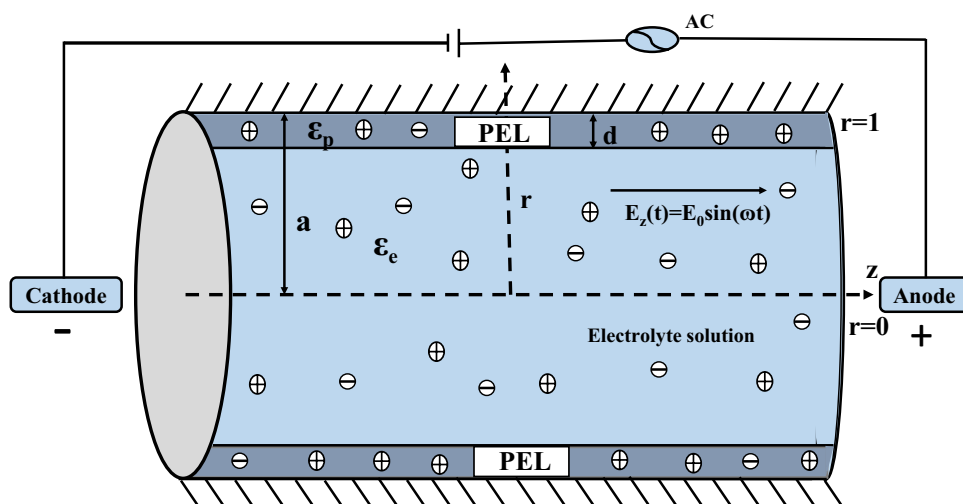
$$\Delta W_i = \frac{(z_i e)^2}{8\pi r_i \epsilon_0} \left(\frac{1}{\epsilon_p} - \frac{1}{\epsilon_e} \right) \tag{2}$$

Here r_i is the radius of the i th ionic species. The flow is considered as axisymmetric and fully developed through the cylindrical nanopore. In this study, we consider cylindrical coordinate systems (r, z) where r denotes the radial direction and z is the axial direction. The externally imposed oscillating electric field, $E_z(t^*)$ along the z -direction is assumed to be $E_z(t^*) = E_0 \sin \omega t^*$ where E_0 is the magnitude, $\omega(= 2\pi\ell)$ is the oscillating frequency of the applied electric field, ℓ is the frequency in kHz and t is the time. The flow is driven by an oscillatory electroosmotic force induced by electric double layer and time-dependent applied AC electric field.

Analytic expression for induced potential

The background salt is assumed to be KCl, for which the hydrated radii of the corresponding ionic species K^+ , Cl^- , H^+ and OH^- are respectively 3.30, 3.32, 2.82 and 3.0 Å [34]. For computational simplicity, it is considered that the hydrated radius of the dissociated ions $r_i(= 3.3)$ Å are all equal which leads $\Delta W_i = \Delta W$ for all i and corresponding partition coefficients in Eq. (1) of the binary symmetric electrolyte ions become the same, i.e., $f_1 = f_2 = f$. The

Fig. 1 The schematic diagram of polyelectrolyte layer-coated canonical nanopore



bulk ionic concentration of the i th ionic species is denoted by n_i^0 . Far away from the charged surface n_i^0 approaches to the bulk concentration n_0 (i.e., $n_+^0 = n_-^0 = n_0$). For low-charge density, the ionic species are considered to follow the equilibrium Boltzmann distribution [35] which remains valid if the frequency of the external electric field is not very high (e.g., less than 1 MHz) [36]. Then the distribution of the ionic species inside and outside of the PEL can be written as:

$$n_i^* = \begin{cases} n_i^0 \exp\left(\frac{-z_i e \phi^*}{k_B T}\right) & 0 \leq r^* < a - d^* \\ n_i^0 \exp\left(\frac{-z_i e \phi^*}{k_B T}\right) \exp\left(-\frac{\Delta W}{k_B T}\right) & a - d^* \leq r^* \leq a. \end{cases} \quad (3)$$

Under the thin Debye layer assumption, the distribution of electrolyte potential within and outside PEL is governed by the Poisson equation which relates the net charge density in EDL due to mobile ions and fixed charged within PEL and expressed as

$$\nabla^2 \Phi^* = \begin{cases} -\frac{\sum z_i e n_i^*}{\epsilon_0 \epsilon_c} & 0 \leq r^* < a - d^* \\ -\frac{\sum z_i e n_i^*}{\epsilon_0 \epsilon_p} \exp\left(-\frac{\Delta W}{k_B T}\right) - \frac{\rho_{\text{fix}}}{\epsilon_0 \epsilon_p} & a - d^* \leq r^* \leq a. \end{cases} \quad (4)$$

Using the Debye–Hückel approximation for low surface charge i.e., $\phi < k_B T/e = 0.025$ V and for symmetric binary electrolyte ($z_+ = -z_- = z$), the Poisson–Boltzmann equation for the induced potential distribution can be linearized and expressed inside and outside of the PEL in the following non-dimensional form as

$$\frac{1}{r} \frac{d}{dr} \left(r \frac{d\phi_e}{dr} \right) = (\kappa a)^2 \phi_e \quad 0 \leq r < 1 - d \quad (5a)$$

$$\frac{1}{r} \frac{d}{dr} \left(r \frac{d\phi_p}{dr} \right) = \frac{1}{\epsilon_r} \left[(\kappa a)^2 \exp(-\Delta w) \phi_p - q_{\text{fix}} \right] \quad 1 - d \leq r \leq 1 \quad (5b)$$

Here, ϵ_r is the ratio of the relative dielectric permittivity of the PEL layer to the bulk electrolyte solution and is given by $\epsilon_r = \epsilon_p/\epsilon_c$. ϕ_e and ϕ_p represent the induced potential in electrolyte and PEL region, respectively. We have taken radius of the nanopore, a as a length scale. We scale potential ϕ^* , ζ^* by thermal potential $\phi_0 (= k_B T/e)$, ionic concentration n_i^* by bulk ionic concentration n_0 and the Born energy ΔW by $k_B T$. The scaled fixed charge density in PEL can be expressed as $q_{\text{fix}} = Ne^2 z Z a^2 / \epsilon_0 \epsilon_c k_B T$. The continuity of electrostatic potential and electric displacement are considered at the interface between the PEL and electrolyte region. The dimensionless boundary condition are given as follows

$$\begin{aligned} \frac{d\phi_e}{dr} \Big|_{r=0} &= 0, & \phi_e \Big|_{r=(1-d)^-} &= \phi_p \Big|_{r=(1-d)^+} \\ \frac{d\phi_e}{dr} \Big|_{r=(1-d)^-} &= \epsilon_r \frac{d\phi_p}{dr} \Big|_{r=(1-d)^+}, & \phi_p \Big|_{r=1} &= \zeta \end{aligned} \quad (6)$$

In the present paper, in order to account for the ion-partitioning effects, we have introduced different relative dielectric permittivities of the PEL and the bulk solution. As a result, on the boundary between the PEL and the surrounding electrolyte solution, the electric field strength is no longer continuous and instead the electric displacement becomes continuous [37]. For the case when the relative dielectric permittivities of the PEL and the bulk solution are equal, this boundary condition becomes the continuity condition of the electric field strength. The solutions of the Poisson equation Eqs. (5a) and (5b), inside and outside PEL with the corresponding above boundary condition given in Eq. (6) are as follows

$$\phi_e = AI_0(\kappa ar) + BK_0(\kappa ar) \quad 0 \leq r < 1 - d \quad (7a)$$

$$\begin{aligned} \phi_p = CI_0 \left(\kappa a \sqrt{\frac{m}{\epsilon_r}} r \right) + DK_0 \left(\kappa a \sqrt{\frac{m}{\epsilon_r}} r \right) \\ + \frac{q_{\text{fix}}}{m(\kappa a)^2} \quad 1 - d \leq r \leq 1 \end{aligned} \quad (7b)$$

here, I_n and K_n are the modified Bessel function of first and second kind of order n and we denote $\exp(-\Delta w)$ as m . The values of the arbitrary constants are specified in Eqs. (7a) and (7b) are given in “Appendix 1”.

Analytic expression for velocity field

The nanopore is assumed to be very long and concentrating the study at the middle region far away from inlet/outlet, the flow is considered as unidirectional and fully developed. For unsteady unidirectional EOF in fully developed generalize Maxwell fluid, the modified Cauchy momentum equation with Darcy–Brinkman term in the exterior and interior PEL can be written as

$$\begin{aligned} \rho \frac{\partial}{\partial t^*} u_e^*(r^*, t^*) &= -\frac{1}{r^*} \frac{\partial}{\partial r^*} (r^* \tau_{rz}^*) + \rho_e^* E_z(t^*) \\ 0 &\leq r^* < a - d^* \end{aligned} \quad (8a)$$

$$\begin{aligned} \rho \frac{\partial}{\partial t^*} u_p^*(r^*, t^*) &= -\frac{1}{r^*} \frac{\partial}{\partial r^*} (r^* \tau_{rz}^*) + \rho_e^* E_z(t^*) - \gamma u_p^*(r^*, t^*) \\ a - d^* &\leq r^* \leq a \end{aligned} \quad (8b)$$

here, u_e^* and u_p^* denote the velocity components in the electrolyte and PEL region respectively. γ is the hydrodynamics frictional coefficient [38] of the PEL. The stress tensor of Maxwell fluid τ_{rz}^* , satisfies the constitutive equation

$$\left(1 + \lambda \frac{\partial}{\partial t^*}\right) \tau_{r,z}^* = -\eta_0 \frac{\partial u^*}{\partial r^*} \tag{9}$$

where λ is the relaxation time [39] and η_0 is the zero-shear-rate viscosity of the fluid. Corresponding boundary conditions are given as

$$\begin{aligned} \frac{\partial u_e^*}{\partial r^*} \Big|_{r^*=0} = 0, \quad u_e^* \Big|_{r^*=(a-d)^-} = u_p^* \Big|_{r^*=(a-d)^+} \\ \frac{\partial u_e^*}{\partial r^*} \Big|_{r^*=(a-d)^-} = \frac{\partial u_p^*}{\partial r^*} \Big|_{r^*=(a-d)^+}, \quad u_p^* \Big|_{r^*=a} = 0 \end{aligned} \tag{10}$$

The velocity field u^* and time t^* are scaled by the Helmholtz–Smoluchowski velocity $U_{HS}(= \epsilon_0 \epsilon_e E_0 \phi_0 / \eta_0)$ and $1/\omega$ respectively. The stress coefficient $\tau_{r,z}^*$ is scaled by $\eta_0 U_{HS}/a$. The oscillating Reynolds number Re_w is defined as $Re_w = \rho \omega a^2 / \eta_0$ which represents as the ratio between the characteristic length scale associate with momentum diffusions length scale. Here, $\nu = \eta_0 / \rho$ is the kinematic viscosity. The non-dimensional parameter $\beta = a / \lambda_0^{-1}$, represents a measure of the friction experienced by the fluid within the polyelectrolyte layer where $\lambda_0^{-1} = \sqrt{\eta_0 / \gamma}$ is the softness degree of the PEL.

To establish the analytic solution for the distribution of the induced potential and axial velocity of the present scenario under the AC electric field, we have considered the electric field and velocity in the following complex form as

$$E_z(t^*) = \text{Im}(E_0 e^{i\omega t^*}) \tag{11}$$

$$u^*(r^*, t^*) = \text{Im}(u_0^*(r^*) e^{i\omega t^*}) \tag{12}$$

where Im denotes the imaginary part of a complex number, and $u_0^*(r^*)$ is the complex amplitude of EOF velocity. The Cauchy momentum equation in the non-dimensional form can be written as

$$\begin{aligned} Re_w \frac{\partial u_e}{\partial t} = -\frac{1}{r} \frac{\partial}{\partial r} (r \tau_{rz}) \\ - (\kappa a)^2 \phi_e \text{Im}(e^{it}) \quad 0 \leq r < 1 - d \end{aligned} \tag{13a}$$

$$\begin{aligned} Re_w \frac{\partial u_p}{\partial t} = -\frac{1}{r} \frac{\partial}{\partial r} (r \tau_{rz}) - (\kappa a)^2 m \phi_p \text{Im}(e^{it}) \\ - \beta^2 u_p \quad 1 - d \leq r \leq 1 \end{aligned} \tag{13b}$$

The simplified dimensionless constitutive equation for Maxwell model is

$$\left(1 + Re_w \lambda_1 \frac{\partial}{\partial t}\right) \tau_{rz} = -\frac{\partial u}{\partial r} \tag{14}$$

Here, $\lambda_1 = \lambda \eta_0 / \rho a^2$ represents the competition between elastic and viscous effects of the fluid, called the Deborah number or elasticity number. The non-dimensional form of

momentum equation inside and outside of the PEL can be written as

$$\begin{aligned} \frac{d^2(u_0)_e}{dr^2} + \frac{1}{r} \frac{d(u_0)_e}{dr} - (u_0)_e (iRe_w - \lambda_1 Re_w^2) \\ = (\kappa a)^2 (1 + i\lambda_1 Re_w) AI_0(\kappa ar) \quad 0 \leq r < 1 - d \end{aligned} \tag{15a}$$

$$\begin{aligned} \frac{d^2(u_0)_p}{dr^2} + \frac{1}{r} \frac{d(u_0)_p}{dr} - (u_0)_p (\beta^2 + (iRe_w - \lambda_1 Re_w^2)) \\ = (\kappa a)^2 m (1 + i\lambda_1 Re_w) * \\ \left[CI_0 \left(\kappa a \sqrt{\frac{m}{\epsilon_r}} r \right) + DK_0 \left(\kappa a \sqrt{\frac{m}{\epsilon_r}} r \right) + \frac{q_{fix}}{(\kappa a)^2 m} \right] \\ 1 - d \leq r \leq 1 \end{aligned} \tag{15b}$$

The corresponding dimensionless boundary conditions are given as

$$\begin{aligned} \frac{d(u_0)_e}{dr} \Big|_{r=0} = 0, \quad (u_0)_e \Big|_{r=(1-d)^-} = (u_0)_p \Big|_{r=(1-d)^+} \\ \frac{d(u_0)_e}{dr} \Big|_{r=(1-d)^-} = \frac{d(u_0)_p}{dr} \Big|_{r=(1-d)^+}, \quad (u_0)_p \Big|_{r=1} = 0 \end{aligned} \tag{16}$$

The solution of Eqs. (15a) and (15b) corresponding to the above boundary conditions Eq. (16) are given by

$$\begin{aligned} (u_0)_e = C_1 I_0 \left(\sqrt{(iRe_w - \lambda_1 Re_w^2)} r \right) \\ + D_1 K_0 \left(\sqrt{(iRe_w - \lambda_1 Re_w^2)} r \right) \\ + GI_0(\kappa ar) \quad 0 \leq r < 1 - d \end{aligned} \tag{17a}$$

$$\begin{aligned} (u_0)_p = C_2 I_0 \left(\sqrt{\beta^2 + (iRe_w - \lambda_1 Re_w^2)} r \right) \\ + D_2 K_0 \left(\sqrt{\beta^2 + (iRe_w - \lambda_1 Re_w^2)} r \right) \\ + MI_0 \left(\kappa a \sqrt{\frac{m}{\epsilon_r}} r \right) + NK_0 \left(\kappa a \sqrt{\frac{m}{\epsilon_r}} r \right) \\ - q_{fix} \frac{1 + i\lambda_1 Re_w}{\beta^2 + (iRe_w - \lambda_1 Re_w^2)} \quad 1 - d \leq r \leq 1 \end{aligned} \tag{17b}$$

The value of the arbitrary constants are specified in Eqs. (17) and (17b) are given in ‘‘Appendix 2’’. We have calculated the dimensional volumetric flow rate per unit width through the nanopore [40] in the following as

$$q_v^* = \int_0^a \frac{u^*(r^*, t^*) 2\pi r^* dr^*}{\pi a^2} \tag{18}$$

Introducing q_v^* as $q_v^* = \text{Im}((q_0^*)_v e^{i\omega t^*})$, then

$$(q_0^*)_v = 2U_{HS}a^2 \int_0^1 u_0(r)rdr \quad (19)$$

We have introduced the scaling factor of the volumetric flow rate as $U_{HS}a^2$. Therefore, the dimensionless volume flow rate is given by

$$(q_0)_v = 2 \int_0^1 u_0(r)rdr \quad (20)$$

Analytic expression for the concentration field

The concentration distribution of the electroneutral solute along the nanopore of length L is studied in the present analysis. Both ends of the nanopore are connected to a large reservoirs which is maintained with uniform concentration of neutral solute. The concentrations of the left and right reservoirs are c_1 and c_2 respectively where $c_1 > c_2$. The species concentration is also considered as infinitely dilute, so that the concentration gradient will not interfere with each other's. In the absence of no chemical reaction or absorption of solute along the nanopore wall, the characteristic behaviour of the species in an isotropic medium is governed by convection–diffusion equation and is given by

$$\frac{\partial c_e^*}{\partial t^*} + u_e^* \frac{\partial c_e^*}{\partial z^*} = D \frac{1}{r^*} \frac{\partial}{\partial r^*} \left(r^* \frac{\partial c_e^*}{\partial r^*} \right) \quad 0 \leq r^* < a - d^* \quad (21a)$$

$$\frac{\partial c_p^*}{\partial t^*} + u_p^* \frac{\partial c_p^*}{\partial z^*} = D \frac{1}{r^*} \frac{\partial}{\partial r^*} \left(r^* \frac{\partial c_p^*}{\partial r^*} \right) \quad a - d^* \leq r^* \leq a \quad (21b)$$

where c_e^* and c_p^* are the concentration of the solute species in the electrolyte region and PEL, respectively. Here, D represents the diffusion coefficient of the solute species in the fluid. The non-uniformity of the velocity distribution will cause that the concentration field is no longer uniform at cross-section of the nanopore. We have considered here Chatwin approximation [41, 42] because of the linearity of Eqs. (21a) and (21b). Therefore, the the concentration field can be expressed as the sum of a linear concentration distribution and a concentration distribution caused by the periodic effect of the velocity field. The species distribution of solute can be written as follow

$$c^*(z^*, r^*, t^*) = c_1 + \frac{c_2 - c_1}{L} z^* + c_0^*(r^*, t^*) \quad (22)$$

where $c_0^*(r^*, t^*)$ denotes the concentration distribution caused by the imposed oscillatory effect of the velocity. The boundary conditions at the two end are considered as

$$\begin{aligned} c^* &= c_1 \quad \text{at} \quad z^* = 0 \\ c^* &= c_2 \quad \text{at} \quad z^* = L \end{aligned} \quad (23)$$

These boundary conditions of the above equation are not satisfied at the end of nanopore due to imposed flow oscillation effect $c_0^*(r^*, t^*)$. But it is observed that such approximation is still valid far from the nanopore ends [42, 43] by neglecting the end effect of a low-aspect-ratio configuration with $a \ll L$.

$$\begin{aligned} \frac{\partial (c_0)_e^*}{\partial t^*} + u_e^* \frac{c_2 - c_1}{L} \\ = D \frac{1}{r^*} \frac{\partial}{\partial r^*} \left(r^* \frac{\partial (c_0)_e^*}{\partial r^*} \right) \quad 0 \leq r^* < a - d^* \end{aligned} \quad (24a)$$

$$\begin{aligned} \frac{\partial (c_0)_p^*}{\partial t^*} + u_p^* \frac{c_2 - c_1}{L} \\ = D \frac{1}{r^*} \frac{\partial}{\partial r^*} \left(r^* \frac{\partial (c_0)_p^*}{\partial r^*} \right) \quad a - d^* \leq r^* \leq a \end{aligned} \quad (24b)$$

The boundary conditions for the above Eqs. (24a) and (24b) are given by

$$\begin{aligned} \frac{\partial (c_0)_e^*}{\partial r^*} \Big|_{r^*=0} = 0, \quad \frac{\partial (c_0)_p^*}{\partial r^*} \Big|_{r^*=(a-d^*)^+} = \frac{\partial (c_0)_e^*}{\partial r^*} \Big|_{r^*=(a-d^*)^-} \\ (c_0)_p^* \Big|_{r^*=(a-d^*)^+} = (c_0)_e^* \Big|_{r^*=(a-d^*)^-} \quad \frac{\partial (c_0)_p^*}{\partial r^*} \Big|_{r^*=a} = 0 \end{aligned} \quad (25)$$

The species concentrations $(c_0)_e^*$ and $(c_0)_p^*$ are scaled by $(c_2 - c_1)$. The species concentration is assumed to be of the form as $c_0(r^*, t^*) = \text{Im}(g^*(r^*)e^{i\omega t^*})$ and accordingly the species conversion equations become

$$\frac{d^2 g_e}{dr^2} + \frac{1}{r} \frac{dg_e}{dr} - i\text{Re}_w \text{Sc} g_e = \varepsilon \text{Pe} u_e \quad 0 \leq r < 1 - d \quad (26a)$$

$$\frac{d^2 g_p}{dr^2} + \frac{1}{r} \frac{dg_p}{dr} - i\text{Re}_w \text{Sc} g_p = \varepsilon \text{Pe} u_p \quad 1 - d \leq r \leq 1 \quad (26b)$$

where g_e and g_p are, respectively, the dimensionless solute concentration in the electrolyte and PEL region. The aspect ratio is denoted as $\varepsilon = a/L$, Schmidt number Sc is defined as $\text{Sc} = \nu/D$ and Pe is the Peclet number and defined by $\text{Pe} = U_{HS}a/D$. The corresponding dimensionless boundary conditions are given as

$$\begin{aligned} \frac{dg_e}{dr} \Big|_{r=0} = 0, \quad \frac{dg_p}{dr} \Big|_{r=(1-d)^+} = \frac{dg_e}{dr} \Big|_{r=(1-d)^-} \\ g_p \Big|_{r=(1-d)^+} = g_e \Big|_{r=(1-d)^-} \quad \frac{dg_p}{dr} \Big|_{r=1} = 0 \end{aligned} \quad (27)$$

The solutions of the above Eqs. (26a) and (26b) corresponding to the boundary conditions Eq. (27) are given by

$$g_e(r) = G_1 I_0(\sqrt{i \text{Re}_w \text{Scr}}) + G_2 K_0(\sqrt{i \text{Re}_w \text{Scr}}) + G_3 I_0(\sqrt{(i \text{Re}_w - \lambda_1 \text{Re}_w^2)r}) + G_4 I_0(\kappa a r) \quad 0 \leq r < 1 - d \tag{28a}$$

$$g_p(r) = G_9 I_0(\sqrt{i \text{Re}_w \text{Scr}}) + G_{10} K_0(\sqrt{i \text{Re}_w \text{Scr}}) + G_5 I_0(\sqrt{\beta^2 + (i \text{Re}_w - \lambda_1 \text{Re}_w^2)r}) + G_6 K_0(\sqrt{\beta^2 + (i \text{Re}_w - \lambda_1 \text{Re}_w^2)r}) + G_7 I_0(\kappa a \sqrt{\frac{m}{\epsilon_r}} r) + G_8 K_0(\kappa a \sqrt{\frac{m}{\epsilon_r}} r) + q_{\text{fix}} \frac{\epsilon(1 + i \lambda_1 \text{Re}_w) \text{Pe}}{i(\beta^2 + (i \text{Re}_w - \lambda_1 \text{Re}_w^2)) \text{Re}_w \text{Sc}} 1 - d \leq r \leq 1 \tag{28b}$$

The value of the arbitrary constants are specified in Eqs. (28a) and (28b) are given in ‘‘Appendix 3’’.

For oscillatory electroosmotic flow, we have introduced the concept of tidal displacement Δz [19, 42]. Basically, tidal displacement represents the average moving distance of each cross section on full cycle of oscillation $T(= 2\pi/\omega)$ [19, 44] and defined as

$$\Delta z = \frac{2}{a^2 \pi} \left| \int_0^a \int_0^T u^* r^* dr^* dt^* \right| \tag{29}$$

When the tidal displacement has to be considered the same value for each flow situation, then the imposed electric field, Helmholtz–Smoluchowski velocity and corresponding Peclet number will no longer remain constant. The Helmholtz–Smoluchowski velocity subjected into Eq. (29) can be redefined as

$$U_{\text{HS}} = \frac{\Delta z \omega}{4 \left| \int_0^1 u_0 r dr \right|} \tag{30}$$

A net mass transport exists from upstream to downstream, due to either the pure diffusion effect or the convective effect. The net mass transport is calculated based on the time and space average mass-transfer rate [19, 44, 45] for each cross-section of the tube in one period of oscillation

$$m_\theta^* = \frac{2}{a^2 T} \int_0^a \int_0^T j_z r^* dr^* dt^* \tag{31}$$

The instant mass flux in the z -direction is denoted by j_z caused due to convection diffusion effects and defined as

$$j_z = -D \frac{c_2 - c_1}{L} + \left(c_1 + \frac{c_2 - c_1}{L} z^* + c_0^*(r^*, t^*) \right) u^* \tag{32}$$

Equivalently,

$$j_z = -D \frac{c_2 - c_1}{L} + c_1 \text{Im}(u_0^* e^{i\omega t^*}) + z^* \frac{c_2 - c_1}{L} \text{Im}(u_0^* e^{i\omega t^*}) + \text{Im}(g^* e^{i\omega t^*}) \text{Im}(u_0^* e^{i\omega t^*}) \tag{33}$$

The dimensionless form of Eq. (33) is given by

$$j_z = -D \frac{c_2 - c_1}{L} + U_{\text{HS}} c_1 \text{Im}(u e^{it}) + a U_{\text{HS}} z \frac{c_2 - c_1}{L} \text{Im}(u_0 e^{it}) + U_{\text{HS}} (c_2 - c_1) \text{Im}(g e^{it}) \text{Im}(u_0 e^{it}) \tag{34}$$

Introducing Eq. (34) in Eq. (31) and express $m_\theta = m_\theta^* L/D(c_1 - c_2)$ as dimensionless average mass transport rate in the following

$$m_\theta = 2 \int_0^1 r dr - 2 \frac{\text{Pe}_w}{\epsilon} \int_0^1 \text{Im}(g e^{it}) \text{Im}(u_0 e^{it}) r dr \tag{35}$$

$$= 2 \int_0^1 r dr - 2 \frac{\text{Pe}_w}{\epsilon} \int_0^1 \text{Re}(u_0 \bar{g}) r dr \tag{36}$$

where $\text{Re}[\cdot]$ denotes the real part of the product of the function u_0 by the complex conjugate of the function g . We have redefined Peclet number based on the angular phenomena as $\text{Pe}_w = \frac{\text{Re}_w \text{Sc} \Delta Z}{| \langle u_0 \rangle |}$ where, $| \langle u_0 \rangle | = | 4 \int_0^1 u_0 r dr |$ and $\Delta Z = \frac{\Delta z}{a}$. The dimensionless induced potential, axial velocity, average fluid velocity, concentration distribution and mass transfer rate have been evaluated numerically with MATLAB [46].

Results

In the previous section, we have established the analytic solution for the distribution of induced potential and axial velocity based on the modified Bessel function. These solutions rely some non-dimensional parameter such as oscillating Reynolds number Re_w , permittivity ratio ϵ_r , normalized relaxation time $\lambda \omega$, Debye–Hückel parameter κa , softness parameter β and nanopore surface charge ζ which control the electrokinetic flow dynamics for the present study. The nanopore wall has fixed zeta potential $\phi^* = \zeta^* = -0.025 \text{ V}$ (i.e. $\zeta = -1$). We have considered the nanopore radius $a = 20 \times 10^{-9} \text{ m}$, the thickness of the PEL $d = 0.2$, permittivity of the electrolyte solution $\epsilon_0 \epsilon_c = 79.8 \times 8.854 \times 10^{12} \text{ F m}^{-1}$, density $\rho = 10^3 \text{ kg/m}^3$, zero shzre rate $\eta_0 = 10^{-3} \text{ kg m}^{-1} \text{ s}^{-1}$, Boltzmann constant $k_B = 1.3806 \times 10^{-23} \text{ J K}^{-1}$, elementary charge

$e = 1.602 \times 10^{-19}$ C, Faraday's constant $F = 96,472$ Cmol⁻¹, aspect ratio $\varepsilon = 0.001$, Peclet number $Pe = 5000$, absolute temperature $T=298$ K, Helmholtz–Smoluchowski velocity $U_{HS} = 0.18158$ m s⁻¹, and applied electric field $E_0=10^7$ V/m. Generally, the parametric values of oscillation frequency in the applied AC electric field is $10 \leq \omega \leq 10^3$ s⁻¹ [39] and relaxation time is $10^{-4} \leq \lambda \leq 10^3$ s [47]. In order to ensure the fundamental assumption for undistributed EDL structure [22, 48] in steady state, the relaxation time λ must be smaller than the imposed oscillating frequency $2\pi/\omega$ [39, 47]. This restriction can be expressed in the dimensionless form as $\lambda_1 Re_w \leq 2\pi$ which implies the normalized relaxation time $\lambda\omega \leq 2\pi$. The variation of fluid velocity with time is one of the most significant characteristics in AC electroosmotic flow in a generalized Maxwell fluids through a nanopore. The instantaneous change in velocity profiles within a period of a time cycle (t varies from 0 to 2π) are illustrated in some profile figures at different scaled time. We have also verified the distribution of the axial velocity of EOF of a Newtonian fluid for a particular case of Maxwell fluid. We analyzed the neutral species transport phenomena through the carrier fluid without effecting the electric potential.

Velocity field and solute transport

Figure 2 depicts the scaled axial velocity and concentration profiles for different values of the Debye–Hückel parameter $\kappa a (= 5, 15, 50)$ when oscillating Reynolds number $Re_w = 5$, permittivity ratio $\varepsilon_r = 0.7$, PEL fixed charge density $q_{fix} = 5$, softness parameter $\beta = 1$. First and second columns correspond to the axial velocity profiles for Newtonian $\lambda = 0$ and Maxwell fluid $\lambda\omega = 5$ respectively while third column indicates the concentration profiles corresponding to the Maxwell fluid $\lambda\omega = 5$. The axial velocity increases with the Debye–Hückel parameter κa i.e., ionic concentration of the electrolyte solution for both Newtonian and Maxwell fluid but it almost remains constant for high ionic concentration. Due to the shearing-thinning effects, the magnitude of the axial velocity for Maxwell fluid is always greater than the Newtonian fluid. It is also noted in Newtonian fluid that the velocity gradient occurs near the nanopore surface wall region. The concentration is also increased with axial velocity for the Maxwell fluid.

The scaled axial velocity and concentration profiles are shown in Fig. 3 for different values of PEL scaled charge density $q_{fix} (= 2, 5, 15)$. The surface potential of the nanopore wall is considered as $\zeta = -1$ while the charge density of the PEL is positive. The increase in positive charge density of the PEL reduces the axial velocity both the Newtonian $\lambda = 0$ (first column) and generalized Maxwell fluid $\lambda\omega = 5$ (second column) for fixed Debye–Hückel parameter $\kappa a = 20$. Here, we considered the oscillating Reynolds number $Re_w = 5$,

permittivity ratio $\varepsilon_r = 0.7$ and softness parameter $\beta = 1$. As shown in third column of Fig. 3, the increasing scaled charge density decreases concentration distribution.

Figure 4 displays the scaled axial velocity and concentration profiles for different values of permittivity ratio $\varepsilon_r (= 0.3, 0.6, 1.0)$ at different dimensionless time for fixed oscillating Reynolds number $Re_w = 5$, PEL scaled fixed charge density $q_{fix} = 5$, Debye–Hückel parameter $\kappa a = 20$ and softness parameter $\beta = 1$. As permittivity ratio ε_r indicates the dielectric permittivity ratio between the PEL layer and the electrolyte solution while $\varepsilon_r = 1$ implies the same permittivity among these two adjacent layer. Due to the low dielectric permittivity of the PEL and the electrolyte solution, low counter ions penetrate in the PEL, as a result the ion-partitioning effects occurs. The axial velocity increases with the permittivity ratios and this effects is more prominent in Maxwell fluid $\lambda\omega = 5$. To analyse the influence of the permittivity ratio in concentration distribution, we plotted the concentration profiles of the generalized Maxwell fluid $\lambda\omega = 5$ in third column of Fig. 4. Similarly as axial velocity, the concentration distribution is also increased with the permittivity ratio.

The effects of variation of softness parameter $\beta (= 1, 3, 5)$ on the axial velocity and concentration profiles are shown in Fig. 5 when the oscillating Reynolds number $Re_w = 5$, permittivity ratio $\varepsilon_r = 0.7$, Debye–Hückel parameter $\kappa a = 20$, PEL scaled fixed charge density $q_{fix} = 5$. The scaled axial velocity decreases with the increase in the softness parameter for Newtonian fluid $\lambda = 0$ (first column) and generalized Maxwell fluid $\lambda\omega = 5$ (second column). The softness parameter mainly represents the frictional forces acting on the electrolyte solution flowing through the PEL, and it mainly effects the hydrodynamics behaviour inside the nanopore while the conductance is not affected crucially by the flow field. It is cleared from Fig. 5 (second and third column) that as axial scaled velocity decreases, the solute concentration is also decreased with the increase in softness parameter.

The oscillating Reynolds numbers have a great impact on the fluid behaviours. To illustrate this effects, we plotted the variation of axial velocity and concentration profiles for different oscillating Reynolds number at different time for both Newtonian and generalized Maxwell fluids case when the permittivity ratio $\varepsilon_r = 0.7$, Debye–Hückel parameter $\kappa a = 20$, PEL scaled fixed charge density $q_{fix} = 5$ and softness parameter $\beta = 1$. For low oscillating Reynolds number, the viscoelasticity of the fluid does not affect the hydrodynamics practice in comparison with the Newtonian fluid (first column) and the axial velocity form plug-like profile shape in both fluids. The magnitude of the axial velocity profile of EOF decreases with the higher values of oscillating Reynolds number where as the flow oscillation increases for the generalized Maxwell fluid $\lambda\omega = 3$ as shown in second column of Fig. 6. The concentration profiles (third column)

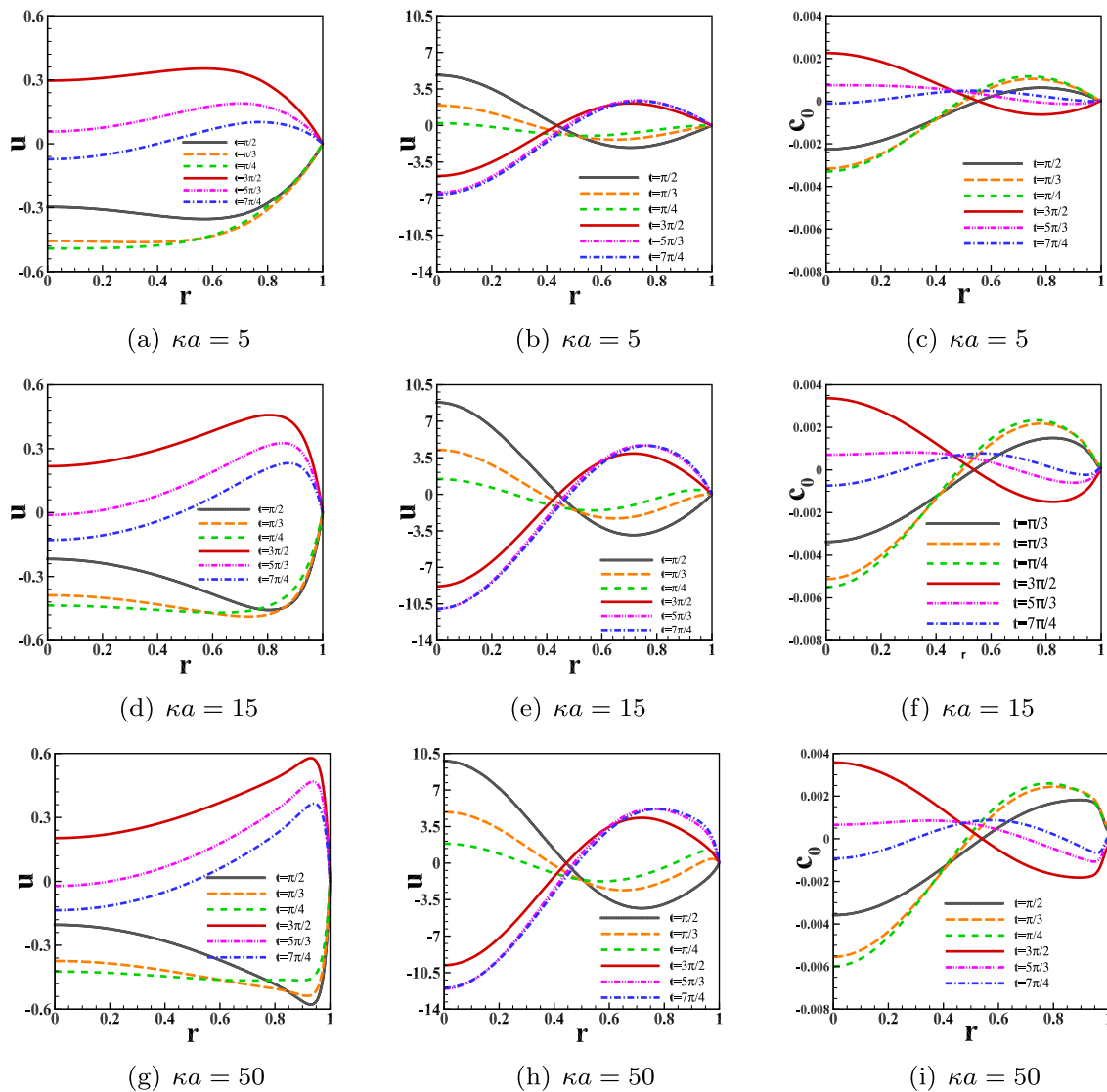


Fig. 2 Distribution of the dimensionless axial velocity profiles of Newtonian fluid $\lambda = 0$ (first column), Maxwell fluid $\lambda\omega = 5$ (second column) and corresponding dimensionless concentration profiles (third column) of the Maxwell fluid $\lambda\omega = 5$ for different values of

Debye–Hückel parameter κa ($= 5, 15, 50$) at different dimensionless time. Here, Schmidt number $Sc = 2000$, oscillating Reynolds number $Re_w = 5$, PEL fixed charge density $q_{fix} = 5$, permittivity ratio $\epsilon_r = 0.7$ and softness parameter $\beta = 1$

corresponding to this Maxwell fluid show that, concentration amplitude decreases but oscillation increases with the higher oscillating Reynolds number.

To show the influence of the normalized relaxation time $\lambda\omega$, we illustrated the distribution of the axial velocity profiles (first row; a, b, c, d) and corresponding distribution of the concentration profiles (second row; e, f, g, h) for different dimensionless time in Fig. 7 when oscillating Reynolds number $Re_w = 15$, permittivity ratio $\epsilon_r = 0.7$, Debye–Hückel parameter $\kappa a = 20$, PEL scaled fixed charge density $q_{fix} = 5$ and softness parameter $\beta = 1$. For the higher value of the oscillating Reynolds number, flow oscillation occurs in both the Newtonian and generalized Maxwell fluids, but

it’s occurrences are more rapid in generalized Maxwell fluid cases. The amplitude of the axial velocity increases with higher values of normalized relaxation time for generalized Maxwell fluids in different time. It is observed that the viscoelastic effects increase the axial fluid velocity due to higher fluidity. Since the oscillation time period is much smaller than the diffusion time scale and hence there is no sufficient time for the flow moment to diffuse away from the nanopore surface. As a result, the effects are only restricted only within a thin layer near the nanopore wall surface. The axial velocity and subsequent concentration distribution corresponding to the Newtonian fluid ($\lambda = 0$) are shown in Fig. 7a and c, respectively. It can be observed from

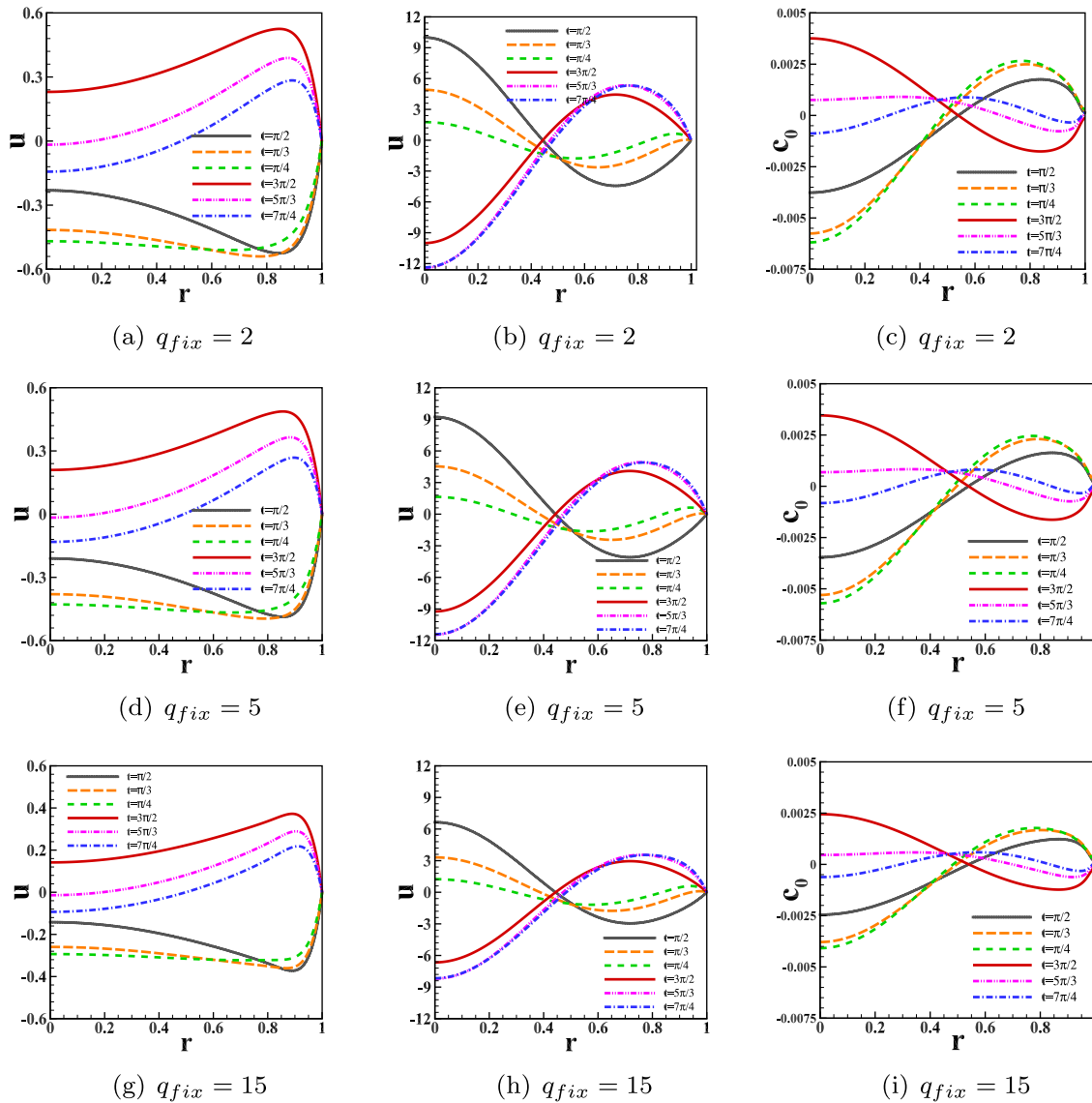


Fig. 3 Distribution of the dimensionless axial velocity profiles of Newtonian fluid $\lambda = 0$ (first column), Maxwell fluid $\lambda\omega = 5$ (second column) and corresponding dimensionless concentration profiles of the Maxwell fluid $\lambda\omega = 5$ for different values of

scaled PEL fixed charge density $q_{fix} (= 2, 5, 15)$ at different dimensionless time. Here, Schmidt number $Sc = 2000$, oscillating Reynolds number $Re_w = 5.0$, Debye–Hückel parameter $\kappa a = 20$, permittivity ratio $\epsilon_r = 0.7$ and softness parameter $\beta = 1$

Fig. 7 that the increasing values of the relaxation time ($\lambda\omega$) enhance both of the solute concentration and oscillation.

Volumetric flow rate, average mass transport and neutralization factor

In Fig. 8, we illustrated the scaled volumetric flow rate (q_0)_v as a function of normalized relaxation times $\lambda\omega$ of Maxwell fluids for different values of permittivity ratio ϵ_r , PEL fixed charge density q_{fix} and oscillating Reynolds number Re_w . The effects of the permittivity ratio on volumetric flow rate is shown in Fig. 8a when the PEL charge density $q_{fix} (= 5)$, Debye–Hückel parameter $\kappa a (= 40)$ and oscillating

Reynolds number $Re_w (= 15)$ are fixed. The volumetric flow rate increases with permittivity ratio between PEL and electrolyte region. It has been shown in Fig. 8b that the scaled volumetric flow rate decreases with the increases of the positive charge density in PEL. We have also plotted the variation of the volumetric flow rate for different oscillating Reynolds number in Fig. 8c and it is observed that volumetric flow rate decreases with higher values of the oscillating Reynolds number. It can be seen from all these in Fig. 8 that the volumetric flow rate has some peaks for some normalized relaxation time. Due to the elasticity, the fluid velocity decreases for some relaxation time and increases for others relaxation time.

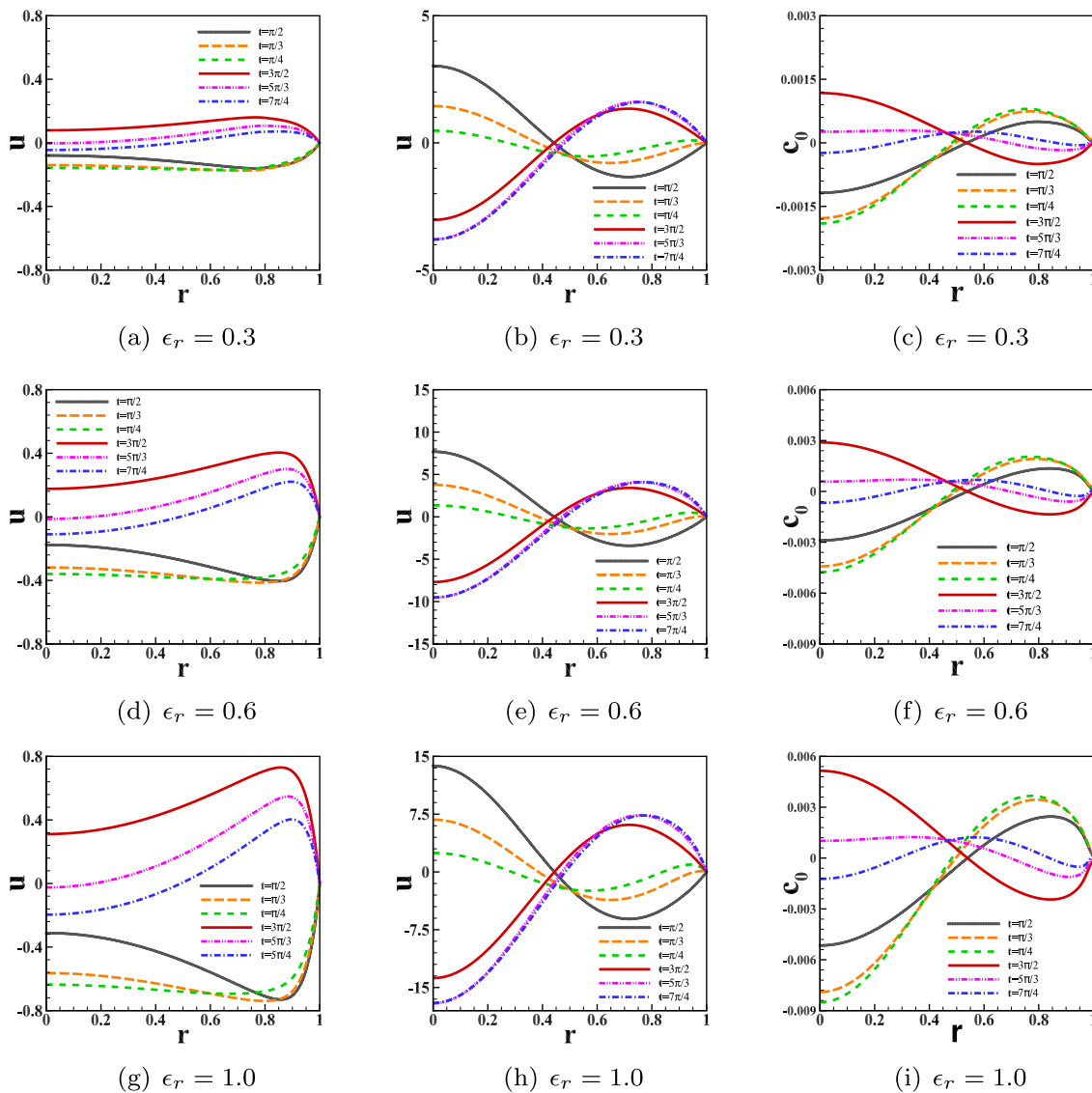


Fig. 4 Distribution of the dimensionless axial velocity profiles of Newtonian fluid $\lambda = 0$ (first column), Maxwell fluid $\lambda\omega = 5$ (second column) and corresponding dimensionless concentration profiles of the Maxwell fluid $\lambda\omega = 5$ for different values of

permittivity ratio ϵ_r ($= 0.3, 0.6, 1.0$) at different dimensionless time. Here, Schmidt number $Sc = 2000$, oscillating Reynolds number $Re_w = 5$, Debye–Hückel parameter $\kappa a = 20$, PEL scaled fixed charge density $q_{fix} = 5$ and softness parameter $\beta = 1$

The dimensionless average mass transport rate m_θ is illustrated in Fig. 9a for different values of the tidal displacement ΔZ when the Schmidt number $Sc = 1000$ and oscillating Reynolds number $Re_w = 15$ for generalized Maxwell fluids. It shows that the mass transport rate increases with normalized relaxation time. The increase in the tidal displacement intensifies the instantaneous convective and dispersion effects in the concentration field and promote the mass transport rate when Schmidt number and oscillating Reynolds number are fixed. To visualize

the reasonable comparison of performance rate of the average mass transport, the tidal displacement ΔZ has considered to be same as ΔZ for each flow situation as shown in Fig. 9b and c. Figure 9b shows that the variation of the average mass transport rate increases with normalized relaxation times for different values of oscillating Reynolds number Re_w ($= 20, 40, 60$) for fixed Schmidt number Sc ($= 1000$) and tidal displacement ΔZ ($= 1.0$). It also shows that the mass transport rate decreases with the increase in the oscillating Reynolds number and it is more prominent

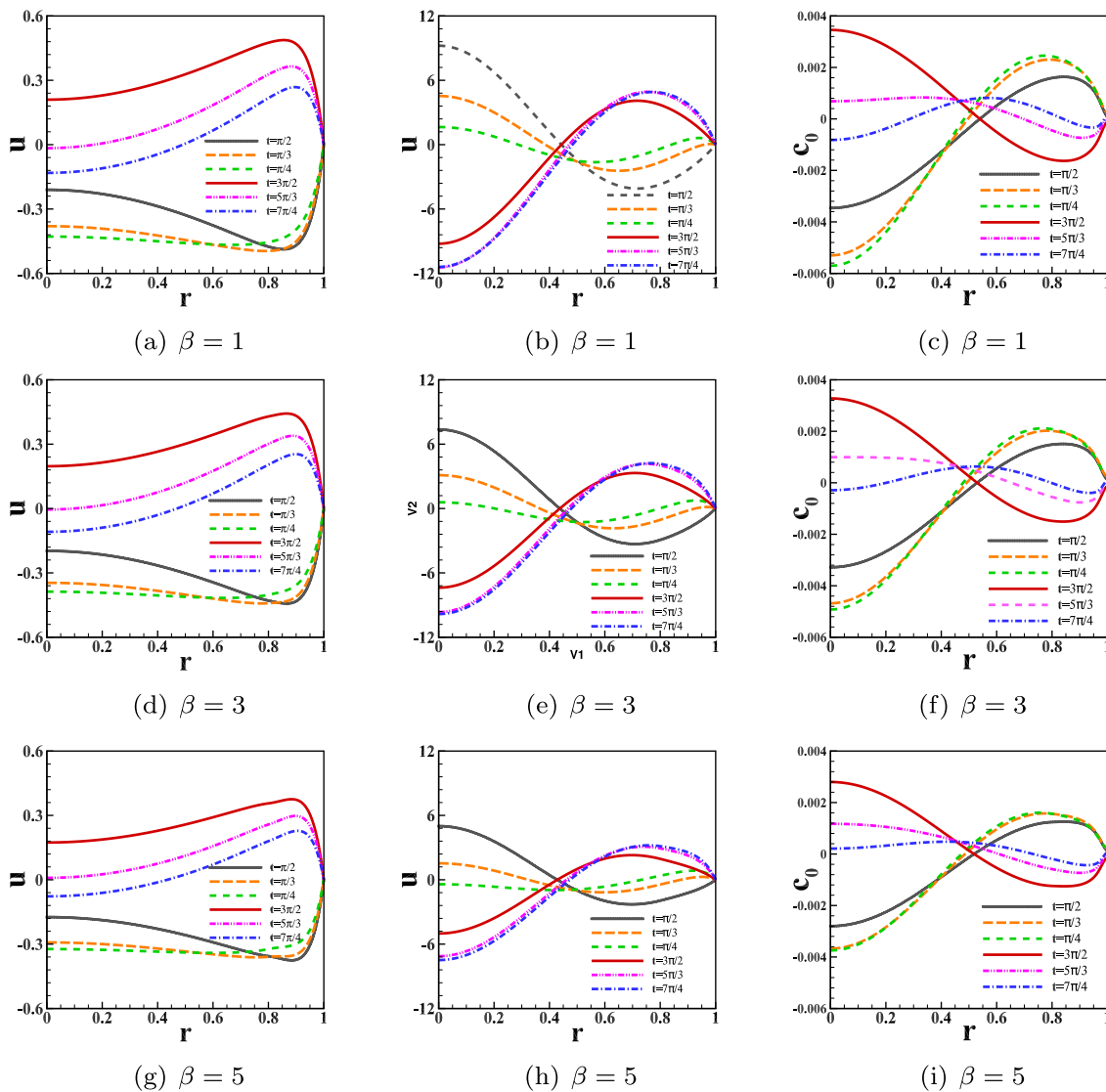


Fig. 5 Distribution of the dimensionless axial velocity profiles of Newtonian fluid $\lambda = 0$ (first column), Maxwell fluid $\lambda\omega = 5$ (second column) and corresponding dimensionless concentration profiles (third column) of the Maxwell fluid $\lambda\omega = 5$ for different values of

softness parameter $\beta (= 1, 3, 5)$ at different dimensionless time. Here, Schmidt number $Sc = 2000$, oscillating Reynolds number $Re_w = 5$, Debye–Hückel parameter $\kappa a = 20$, permittivity ratio $\epsilon_r = 0.7$ and PEL scaled fixed charge density $q_{fix} = 5$

in higher values of the normalized relaxation time. The influence of Schmidt number on average mass transport rate is illustrated in Fig. 9c for fixed oscillating Reynolds number $Re_w (= 15)$ and tidal displacement $\Delta Z (= 1)$. It is shown from this figure that the increase in Schmidt number enhance the mass transport rate. For small mass, diffusivity implies large Schmidt number Sc which enhance the average mass transport rate and oscillatory EOF is more effective to intensify mass transport rate for large Schmidt number.

To demonstrate the charge neutralization in PEL, we have calculated the neutralization factor Γ [49] and is defined as

$$\Gamma = 1 - \frac{Q_{eff}}{Q_{fix}} \tag{37}$$

where Q_{eff} is the volume average effective charge density and defined as

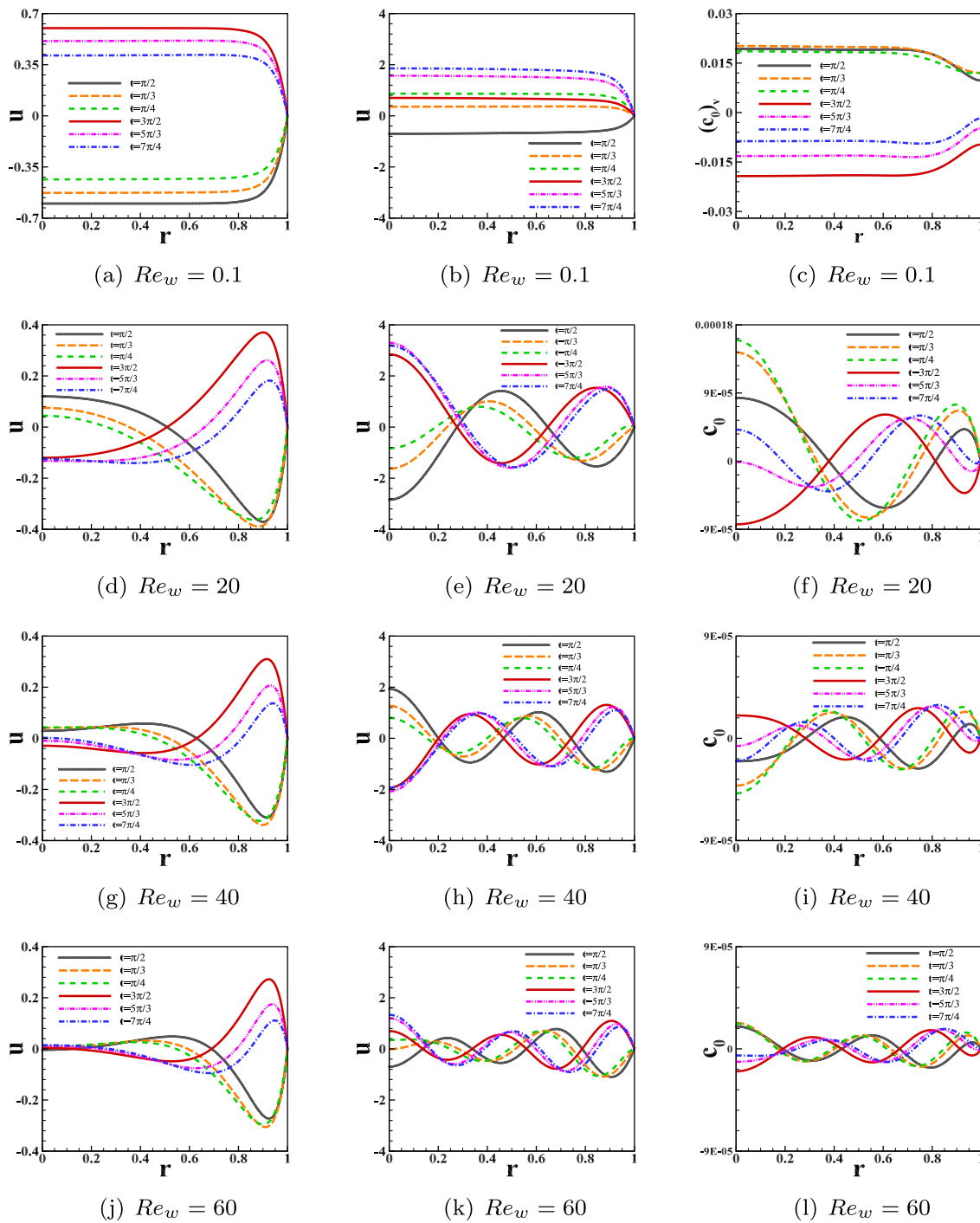


Fig. 6 Distribution of the dimensionless axial velocity profiles of Newtonian fluid $\lambda = 0$ (first column), Maxwell fluid $\lambda\omega = 3$ (second column) and corresponding dimensionless concentration profiles of the Maxwell fluid $\lambda\omega = 3$ for different

values of oscillating Reynolds number $Re_w (= 0.1, 20, 40, 60)$ at different dimensionless time. Here, Schmidt number $Sc = 2000$, Debye–Hückel parameter $\kappa a = 20$, permittivity ratio $\epsilon_r = 0.7$, PEL scaled fixed charge density $q_{fix} = 5$ and softness parameter $\beta = 1$

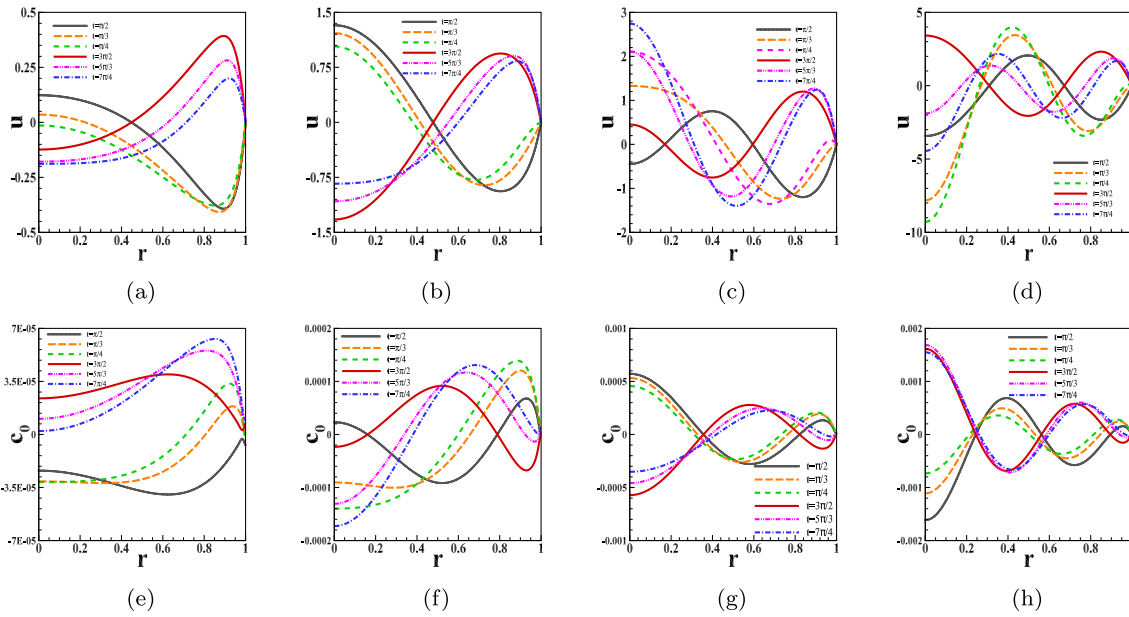


Fig. 7 Distribution of **a** dimensionless axial velocity profiles (first row) and **b** corresponding dimensionless concentration profiles (second row) for different values of normalized relaxation time $\lambda\omega$ ($= 0, 1.5, 3.0, 6.0$) at different dimensionless time. Here, Schmidt

number $Sc = 2000$, oscillating Reynolds number $Re_w = 15$, Debye–Hückel parameter $\kappa a = 20$, permittivity ratio $\epsilon_r = 0.7$, PEL scaled fixed charge density $q_{fix} = 5$ and softness parameter $\beta = 1$

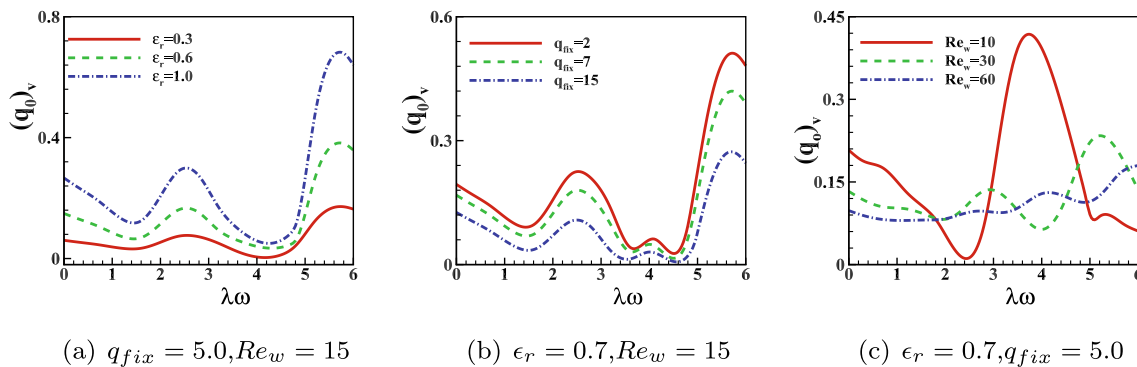


Fig. 8 Variation of volumetric flow rate $(q_0)_v$ with different value of normalized relaxation time $\lambda\omega$ of Maxwell fluid corresponding to different values of **a** permittivity ratio ϵ_r , **b** PEL scaled charge density

q_{fix} and **c** oscillating Reynolds number Re_w . Here, Debye–Hückel parameter $\kappa a = 40$ and softness parameter $\beta = 1$

$$Q_{eff} = \frac{2}{\omega T} \int_0^1 \int_0^{2\pi} [(ka)^2 \exp(\Delta w_i) \phi + q_{fix}] r dr dt \quad (38)$$

$$Q_{fix} = \frac{2}{\omega T} \int_0^1 \int_0^{2\pi} q_{fix} r dr dt \quad (39)$$

and Q_{fix} signifies the volume average fixed charge density and defined as

Figure 10a shows the variation of the neutralization factor with Debye–Hückel parameter κa (ionic concentration of the electrolyte) for different values of permittivity ratio ϵ_r ,

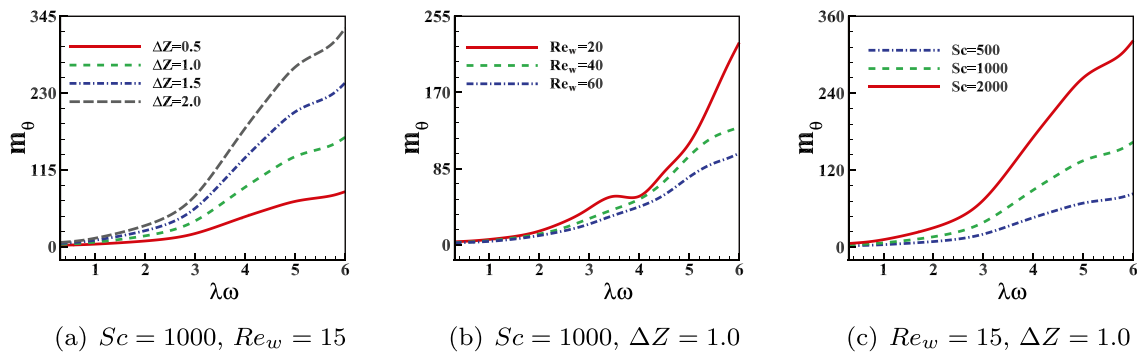
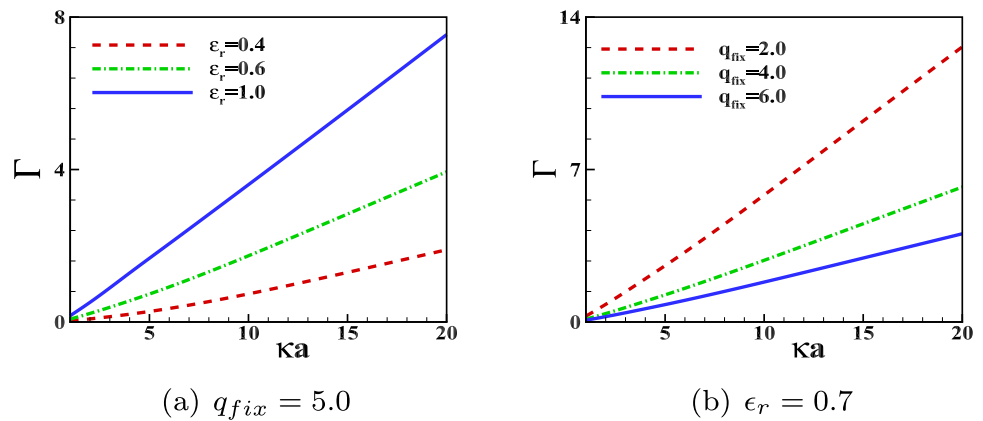


Fig. 9 Variation of dimensionless average mass transport rate m_θ with normalized relaxation time $\lambda\omega$ corresponding to different values of **a** tidal displacement ΔZ **b** oscillating Reynolds number Re_w and **c**

Schmidt number Sc . Here, Debye–Hückel parameter $\kappa a = 20$, permittivity ratio $\epsilon_r = 0.7$, PEL scaled charge density $q_{fix} = 5$ and softness parameter $\beta = 1$

Fig. 10 Variation of the neutralization factor Γ with Debye–Hückel parameters κa of Maxwell fluids $\lambda\omega = 5$ for different values of **a** permittivity ratio ϵ_r and **b** PEL scaled charge density q_{fix} . Here, oscillating Reynolds number $Re_w = 5$ and softness parameter $\beta = 1$



for Maxwell fluids $\lambda\omega = 5$ when oscillating Reynolds number $Re_w = 5$, PEL fixed charge density $q_{fix} = 5$ and softness parameter $\beta = 1$. The charge neutralization factor Γ increases with the Debye–Hückel parameter κa and it attains higher values when the permittivity between the PEL and electrolyte region are same, i.e., $\epsilon_r = 1$ as shown in Fig. 10a. This indicates that the neutralization of immobile charge occurs at a lower rate when the permittivity ratio is small in the PEL. The variation of the neutralization factor Γ with Debye–Hückel parameter κa is illustrated in Fig. 10b for different values of PEL fixed charge density q_{fix} for Maxwell fluids $\lambda\omega = 5$ when oscillating Reynolds number $Re_w = 5$, permittivity ratio $\epsilon_r = 0.7$ and softness parameter $\beta = 1$. In Fig. 10b, it indicates

that the neutralization factor Γ decreases with increases of the positive fixed charge density q_{fix} in PEL but increases with Debye–Hückel parameter κa i.e., ionic concentration of the electrolyte.

Conclusion

The motivation of the present study is to analyse the electrokinetic effects and solute transport phenomena for Maxwell fluids through the polyelectrolyte grafted nanopore considering ion-partitioning effects under AC electric field. Using Debye–Hückel approximation for linearizing modified Poisson–Boltzmann equation, an

analytic expression for induced potential equation was established in the interior and exterior of the PEL. The analytic expression for axial velocity was also presented from the Cauchy momentum equation along with Maxwell constitutive equation in the interior and exterior of the PEL. The axial velocity increases with ionic concentration of the electrolyte solution but it decreases with the increase in the fixed positive charge density in the PEL for both Newtonian and Maxwell fluids cases. The increase in the permittivity ratio enhances the axial velocity for both fluids but its effects are more prominent in Maxwell fluids. The velocity decreases with the increase in the softness parameter. The analytic solution for the convection-diffusions equation was also established in full domain. For higher values of the relaxation time, the axial velocity, and species concentration are both increased. The higher values of the oscillating Reynolds number increase the flow oscillation, as a result the axial velocity decreases. The volumetric flow rate decreases with the increase in the oscillatory Reynolds number and PEL fixed positive charge density but increases with permittivity ratio and relaxation time. For Maxwell fluids, it is also noticed the undulatory distribution in axial velocity and concentration field in comparison to the Newtonian fluids. The average mass transport rate increases with tidal displacement for fixed Schmidt number and relaxation time. The average mass transport rate increases with Schmidt number as well as relaxation time. The neutralization factor increases with permittivity ratio and decreases with PEL fixed charge density.

Appendix 1

Arbitrary constants which are used in the expression (Eqs. 7a and 7b) for the solution of the induced potential equation can be expressed as

$$A = \left(\frac{q_{\text{fix}}}{(\kappa a)^2 m} + F - \frac{ES}{Q} \right) \left(\frac{Q}{QR - PS} \right)$$

$$B = 0$$

$$C = \left(\frac{q_{\text{fix}}}{(\kappa a)^2 m} + F - \frac{ER}{P} \right) \left(\frac{P}{QR - PS} \right)$$

$$D = \frac{1}{k_0 \left(\kappa a \sqrt{\frac{m}{\epsilon_r}} \right)} \left[\zeta - \frac{q_{\text{fix}}}{(\kappa a)^2 m} - CI_0 \left(\kappa a \sqrt{\frac{m}{\epsilon_r}} \right) \right]$$

where the variables can be written as

$$P = I_1(\kappa a(1-d))$$

$$Q = \sqrt{m\epsilon_r} I_1 \left(\kappa a \sqrt{\frac{m}{\epsilon_r}} (1-d) \right) + \frac{I_0 \left(\kappa a \sqrt{\frac{m}{\epsilon_r}} \right)}{K_0 \left(\kappa a \sqrt{\frac{m}{\epsilon_r}} \right)} K_1 \left(\kappa a \sqrt{\frac{m}{\epsilon_r}} (1-d) \right)$$

$$R = I_0(\kappa a(1-d))$$

$$S = I_0 \left(\kappa a \sqrt{\frac{m}{\epsilon_r}} (1-d) \right) - \left(\frac{I_0 \left(\kappa a \sqrt{\frac{m}{\epsilon_r}} \right)}{K_0 \left(\kappa a \sqrt{\frac{m}{\epsilon_r}} \right)} \right) K_0 \left(\kappa a \sqrt{\frac{m}{\epsilon_r}} (1-d) \right)$$

$$E = -\sqrt{m\epsilon_r} \frac{K_1 \left(\kappa a \sqrt{\frac{m}{\epsilon_r}} (1-d) \right)}{K_0 \left(\kappa a \sqrt{\frac{m}{\epsilon_r}} \right)} \left[\zeta - \frac{q_{\text{fix}}}{(\kappa a)^2 m} \right]$$

$$F = \frac{K_0 \left(\kappa a \sqrt{\frac{m}{\epsilon_r}} (1-d) \right)}{K_0 \left(\kappa a \sqrt{\frac{m}{\epsilon_r}} \right)} \left[\zeta - \frac{q_{\text{fix}}}{((\kappa a)^2 m)} \right]$$

Appendix 2

Arbitrary constants which are used in the expression (Eqs. 17 and 17b) of the solution in the momentum equation can be expressed as

$$C_1 = \frac{M_{10}M_7 - M_4M_9}{M_3M_7 - M_4M_6}$$

$$C_2 = \frac{M_6M_{10} - M_9M_3}{M_3M_7 - M_4M_6}$$

$$D_1 = 0$$

$$D_2 = -C_2 \frac{I_0 \left(\sqrt{\beta^2 + (i\text{Re}_w - \lambda_1 \text{Re}_w^2)} \right)}{K_0 \left(\sqrt{\beta^2 + (i\text{Re}_w - \lambda_1 \text{Re}_w^2)} \right)} - \frac{M_2}{K_0 \left(\sqrt{\beta^2 + (i\text{Re}_w - \lambda_1 \text{Re}_w^2)} \right)}$$

where the variables are expressed as

$$\begin{aligned}
 G &= A(\kappa a)^2 \frac{1 + i\lambda_1 \text{Re}_w}{(\kappa a)^2 - (i\text{Re}_w - \lambda_1 \text{Re}_w^2)} \\
 M &= C(\kappa a)^2 m \epsilon_r \frac{1 + i\lambda_1 \text{Re}_w}{(\kappa a)^2 m - \epsilon_r (\beta^2 + (i\text{Re}_w - \lambda_1 \text{Re}_w^2))} \\
 N &= D(\kappa a)^2 m \epsilon_r \frac{1 + i\lambda_1 \text{Re}_w}{(\kappa a)^2 m - \epsilon_r (\beta^2 + (i\text{Re}_w - \lambda_1 \text{Re}_w^2))} \\
 M_2 &= MI_0 \left(\kappa a \sqrt{\frac{m}{\epsilon_r}} \right) + NK_0 \left(\kappa a \sqrt{\frac{m}{\epsilon_r}} \right) \\
 &\quad - q_{\text{fix}} \frac{1 + i\lambda_1 \text{Re}_w}{\beta^2 + (i\text{Re}_w - \lambda_1 \text{Re}_w^2)} \\
 M_3 &= I_0 \left(\sqrt{i\text{Re}_w - \lambda_1 \text{Re}_w^2} (1 - d) \right) \\
 M_4 &= I_0 \left(\sqrt{\beta^2 + (i\text{Re}_w - \lambda_1 \text{Re}_w^2)} (1 - d) \right) \\
 &\quad - \frac{I_0 \left(\sqrt{\beta^2 + (i\text{Re}_w - \lambda_1 \text{Re}_w^2)} \right)}{K_0 \left(\sqrt{\beta^2 + (i\text{Re}_w - \lambda_1 \text{Re}_w^2)} \right)} \\
 &\quad * K_0 \left(\sqrt{\beta^2 + (i\text{Re}_w - \lambda_1 \text{Re}_w^2)} (1 - d) \right) \\
 M_5 &= MI_0 \left(\kappa a \sqrt{\frac{m}{\epsilon_r}} (1 - d) \right) + NK_0 \left(\kappa a \sqrt{\frac{m}{\epsilon_r}} (1 - d) \right) \\
 &\quad - q_{\text{fix}} \frac{1 + i\lambda_1 \text{Re}_w}{\beta^2 + (i\text{Re}_w - \lambda_1 \text{Re}_w^2)} \\
 M_6 &= \sqrt{i\text{Re}_w - \lambda_1 \text{Re}_w^2} I_1 \left(\sqrt{i\text{Re}_w - \lambda_1 \text{Re}_w^2} (1 - d) \right) \\
 M_7 &= \sqrt{\beta^2 + (i\text{Re}_w - \lambda_1 \text{Re}_w^2)} I_1 \\
 &\quad \left(\sqrt{\beta^2 + (i\text{Re}_w - \lambda_1 \text{Re}_w^2)} (1 - d) \right) \\
 &\quad + \frac{I_0 \left(\sqrt{\beta^2 + (i\text{Re}_w - \lambda_1 \text{Re}_w^2)} \right)}{K_0 \left(\sqrt{\beta^2 + (i\text{Re}_w - \lambda_1 \text{Re}_w^2)} \right)} \sqrt{\beta^2 + (i\text{Re}_w - \lambda_1 \text{Re}_w^2)} \\
 &\quad * K_1 \left(\sqrt{\beta^2 + (i\text{Re}_w - \lambda_1 \text{Re}_w^2)} (1 - d) \right) \\
 M_8 &= \kappa a \sqrt{\frac{m}{\epsilon_r}} \left(MI_1 \left(\kappa a \sqrt{\frac{m}{\epsilon_r}} (1 - d) \right) \right. \\
 &\quad \left. - NK_1 \left(\kappa a \sqrt{\frac{m}{\epsilon_r}} (1 - d) \right) \right) \\
 M_9 &= \frac{M_2 \sqrt{\beta^2 + (i\text{Re}_w - \lambda_1 \text{Re}_w^2)}}{K_0 \left(\sqrt{\beta^2 + (i\text{Re}_w - \lambda_1 \text{Re}_w^2)} \right)} \\
 &\quad K_1 \left(\sqrt{\beta^2 + (i\text{Re}_w - \lambda_1 \text{Re}_w^2)} (1 - d) \right) \\
 &\quad + M_8 - \kappa a GI_1 (\kappa a (1 - d)) \\
 M_{10} &= M_5 - \frac{M_2}{K_0 \left(\sqrt{\beta^2 + (i\text{Re}_w - \lambda_1 \text{Re}_w^2)} \right)} \\
 &\quad K_0 \left(\sqrt{\beta^2 + (i\text{Re}_w - \lambda_1 \text{Re}_w^2)} (1 - d) \right) \\
 &\quad - GI_0 (\kappa a (1 - d))
 \end{aligned}$$

Appendix 3

Arbitrary constants which are used in the expression (Eqs. 28a and 28b) for the solution of the solute concentration equation can be expressed as

$$\begin{aligned}
 G_1 &= \frac{Z_{13}Z_{15} - Z_{12}Z_{16}}{Z_{11}Z_{15} - Z_{12}Z_{14}} \\
 G_2 &= 0 \\
 G_3 &= F_{13}C_1 \\
 G_4 &= F_{11}G \\
 G_5 &= F_{14}C_2 \\
 G_6 &= F_{14}D_2 \\
 G_7 &= F_{12}M \\
 G_8 &= F_{12}N \\
 G_9 &= -\frac{Y_{21}}{\sqrt{i\text{Re}_w \text{Sc}}} \frac{1}{I_1(\sqrt{i\text{Re}_w \text{Sc}})} + G_{10} \frac{K_1(\sqrt{i\text{Re}_w \text{Sc}})}{I_1(\sqrt{i\text{Re}_w \text{Sc}})} \\
 G_{10} &= \frac{Z_{13}Z_{14} - Z_{11}Z_{16}}{Z_{11}Z_{15} - Z_{12}Z_{14}} \\
 G_{11} &= \frac{\sqrt{i\text{Re}_w - \lambda_1 \text{Re}_w^2}}{\kappa a} \\
 G_{12} &= \frac{\sqrt{\beta^2 + (i\text{Re}_w - \lambda_1 \text{Re}_w^2)}}{\kappa a \sqrt{\frac{m}{\epsilon_r}}}
 \end{aligned}$$

where variables as considered in the following are

$$F_{11} = \frac{\epsilon \text{Pe}}{(\kappa a)^2 - i \text{Re}_w \text{Sc}}$$

$$F_{12} = \frac{\epsilon_r \epsilon \text{Pe}}{(\kappa a)^2 m - i \epsilon_r \text{Re}_w \text{Sc}}$$

$$F_{13} = \frac{\epsilon \text{Pe}}{(\kappa a)^2 G_{11}^2 - i \text{Re}_w \text{Sc}}$$

$$F_{14} = \frac{\epsilon_r \epsilon \text{Pe}}{(\kappa a)^2 m G_{12}^2 - i \epsilon_r \text{Re}_w \text{Sc}}$$

$$Y_{21} = \sqrt{\beta^2 + (i \text{Re}_w - \lambda_1 \text{Re}_w^2) G_5 I_1} \\ \left(\sqrt{\beta^2 + (i \text{Re}_w - \lambda_1 \text{Re}_w^2)} \right) \\ - \sqrt{\beta^2 + (i \text{Re}_w - \lambda_1 \text{Re}_w^2) G_6 K_1} \\ \left(\sqrt{\beta^2 + (i \text{Re}_w - \lambda_1 \text{Re}_w^2)} \right) \\ + \kappa a \sqrt{\frac{m}{\epsilon_r}} \left(G_7 I_1 \left(\kappa a \sqrt{\frac{m}{\epsilon_r}} \right) - G_8 K_1 \left(\kappa a \sqrt{\frac{m}{\epsilon_r}} \right) \right)$$

$$Y_{22} = \sqrt{\beta^2 + (i \text{Re}_w - \lambda_1 \text{Re}_w^2) G_5 I_1} \\ \left(\sqrt{\beta^2 + (i \text{Re}_w - \lambda_1 \text{Re}_w^2)} (1-d) \right) \\ - \sqrt{\beta^2 + (i \text{Re}_w - \lambda_1 \text{Re}_w^2) G_6 K_1} \\ \left(\sqrt{\beta^2 + (i \text{Re}_w - \lambda_1 \text{Re}_w^2)} (1-d) \right) \\ + \kappa a \sqrt{\frac{m}{\epsilon_r}} \left(G_7 I_1 \left(\kappa a \sqrt{\frac{m}{\epsilon_r}} (1-d) \right) \right. \\ \left. - G_8 K_1 \left(\kappa a \sqrt{\frac{m}{\epsilon_r}} (1-d) \right) \right)$$

$$Y_{23} = \sqrt{i \text{Re}_w - \lambda_1 \text{Re}_w^2} G_3 I_1 \left(\sqrt{i \text{Re}_w - \lambda_1 \text{Re}_w^2} (1-d) \right) \\ + \kappa a G_4 I_1 (\kappa a (1-d))$$

$$Y_{24} = Y_{21} \left(\frac{I_1 \left(\sqrt{i \text{Re}_w \text{Sc}} (1-d) \right)}{I_1 \left(\sqrt{i \text{Re}_w \text{Sc}} \right)} \right)$$

$$Y_{25} = G_3 I_0 \left(\sqrt{\beta^2 + (i \text{Re}_w - \lambda_1 \text{Re}_w^2)} (1-d) \right) \\ + G_6 K_0 \left(\sqrt{\beta^2 + (i \text{Re}_w - \lambda_1 \text{Re}_w^2)} (1-d) \right) \\ + G_7 I_0 \left(\kappa a \sqrt{\frac{m}{\epsilon_r}} (1-d) \right) + G_8 K_0 \left(\kappa a \sqrt{\frac{m}{\epsilon_r}} (1-d) \right) \\ + q_{\text{fix}} \frac{\epsilon (1 + i \lambda_1 \text{Re}_w) \text{Pe}}{i (\beta^2 + (i \text{Re}_w - \lambda_1 \text{Re}_w^2)) \text{Re}_w \text{Sc}}$$

$$Y_{26} = G_3 I_0 \left(\sqrt{i \text{Re}_w - \lambda_1 \text{Re}_w^2} (1-d) \right) + G_4 I_0 (\kappa a (1-d))$$

$$Y_{27} = \frac{Y_{21}}{\sqrt{i \text{Re}_w \text{Sc}}} \left(\frac{I_0 \left(\sqrt{i \text{Re}_w \text{Sc}} (1-d) \right)}{I_1 \left(\sqrt{i \text{Re}_w \text{Sc}} \right)} \right)$$

$$Z_{11} = \sqrt{i \text{Re}_w \text{Sc}} I_1 \left(\sqrt{i \text{Re}_w \text{Sc}} (1-d) \right)$$

$$Z_{12} = \sqrt{i \text{Re}_w \text{Sc}} \left[\left(\frac{K_1 \left(\sqrt{i \text{Re}_w \text{Sc}} \right)}{I_1 \left(\sqrt{i \text{Re}_w \text{Sc}} \right)} \right) I_1 \left(\sqrt{i \text{Re}_w \text{Sc}} (1-d) \right) \right. \\ \left. - K_1 \left(\sqrt{i \text{Re}_w \text{Sc}} (1-d) \right) \right]$$

$$Z_{13} = Y_{22} - Y_{23} - Y_{24}$$

$$Z_{14} = I_0 \left(\sqrt{i \text{Re}_w \text{Sc}} (1-d) \right)$$

$$Z_{15} = \left[\left(\frac{K_1 \left(\sqrt{i \text{Re}_w \text{Sc}} \right)}{I_1 \left(\sqrt{i \text{Re}_w \text{Sc}} \right)} \right) I_0 \left(\sqrt{i \text{Re}_w \text{Sc}} (1-d) \right) \right. \\ \left. + K_0 \left(\sqrt{i \text{Re}_w \text{Sc}} (1-d) \right) \right]$$

$$Z_{16} = Y_{25} - Y_{26} - Y_{27}$$

Acknowledgements One of the authors (S. Bera) acknowledges the Science & Engineering Research Board (SERB), Government of India, for providing the financial support through the project grant (File no: ECR/2016/000771).

Authors' contributions All authors read and approved the final manuscript.

Declarations

Competing interests The authors declare no competing interests.

References

- Li L, Yang C, Shi H, Liao W-C, Huang H, Lee LJ, Castro JM, Yi AY (2010) Design and fabrication of an affordable polymer micromixer for medical and biomedical applications. *Polym Eng Sci* 50(8):1594–1604
- Minerick AR (2008) The rapidly growing field of micro and nanotechnology to measure living cells. *AIChE J* 54(9):2230–2237
- Kwak R, Kim SJ, Han J (2011) Continuous-flow biomolecule and cell concentrator by ion concentration polarization. *Anal Chem* 83(19):7348–7355
- Malecha K, Golonka LJ, Bałdyga J, Jasińska M, Sobieszuk P (2009) Serpentine microfluidic mixer made in LTCC. *Sens Actuators B Chem* 143(1):400–413
- Saeed OO, Li R, Deng Y et al (2014) Microfluidic approaches for cancer cell separation. *J Biomed Sci Eng* 7(12):1005
- Das S, Das T, Chakraborty S (2006) Analytical solutions for the rate of DNA hybridization in a microchannel in the presence of pressure-driven and electroosmotic flows. *Sens Actuators B Chem* 114(2):957–963
- Kim SJ, Ko SH, Kang KH, Han J (2010) Direct seawater desalination by ion concentration polarization. *Nat Nanotechnol* 5(4):297–301
- Gencoglu A, Minerick AR (2014) Electrochemical detection techniques in micro- and nanofluidic devices. *Microfluidics Nanofluidics* 17(5):781–807
- Probstein RF (2005) *Physicochemical hydrodynamics: an introduction*. Wiley, Hoboken
- Conlisk A, McFerran J, Zheng Z, Hansford D (2002) Mass transfer and flow in electrically charged micro- and nanochannels. *Anal Chem* 74(9):2139–2150
- Levine S, Marriotti J, Neale G, Epstein N (1975) Theory of electrokinetic flow in fine cylindrical capillaries at high zeta-potentials. *J Colloid Interface Sci* 52(1):136–149
- Wang C-Y, Liu Y-H, Chang CC (2008) Analytical solution of electro-osmotic flow in a semicircular microchannel. *Phys Fluids* 20(6):063105
- Tsao H-K (2000) Electroosmotic flow through an annulus. *J Colloid Interface Sci* 225(1):247–250
- Bianchi F, Ferrigno R, Girault H (2000) Finite element simulation of an electroosmotic-driven flow division at a T-junction of microscale dimensions. *Anal Chem* 72(9):1987–1993
- Bera S, Bhattacharyya S (2018) Effects of geometric modulation and surface potential heterogeneity on electrokinetic flow and solute transport in a microchannel. *Theor Comput Fluid Dyn* 32(2):201–214

16. Dutta P, Beskok A (2001) Analytical solution of time periodic electroosmotic flows: analogies to stokes second problem. *Anal Chem* 73(21):5097–5102
17. Chakraborty S, Ray S (2008) Mass flow-rate control through time periodic electro-osmotic flows in circular microchannels. *Phys Fluids* 20(8):083602
18. Jian Y, Yang L, Liu Q (2010) Time periodic electro-osmotic flow through a microannulus. *Phys Fluids* 22(4):042001
19. Huang H-F, Lai C-L (2006) Enhancement of mass transport and separation of species by oscillatory electroosmotic flows. *Proc R Soc A Math Phys Eng Sci* 462(2071):2017–2038
20. Li F, Jian Y, Chang L, Zhao G, Yang L (2016) Alternating current electroosmotic flow in polyelectrolyte-grafted nanochannel. *Colloids Surf B Biointerfaces* 147:234–241
21. Yeh L-H, Zhang M, Qian S, Hsu J-P, Tseng S (2012) Ion concentration polarization in polyelectrolyte-modified nanopores. *J Phys Chem C* 116(15):8672–8677
22. Li F, Jian Y, Xie Z, Liu Y, Liu Q (2017) Transient alternating current electroosmotic flow of a Jeffrey fluid through a polyelectrolyte-grafted nanochannel. *RSC Adv* 7(2):782–790
23. Chen G, Das S (2015) Electroosmotic transport in polyelectrolyte-grafted nanochannels with pH-dependent charge density. *J Appl Phys* 117(18):185304
24. Lee BP, Messersmith PB, Israelachvili JN, Waite JH (2011) Mussel-inspired adhesives and coatings. *Ann Rev Mater Res* 41:99–132
25. Poddar A, Maity D, Bandopadhyay A, Chakraborty S (2016) Electrokinetics in polyelectrolyte grafted nanofluidic channels modulated by the ion partitioning effect. *Soft Matter* 12(27):5968–5978
26. Ganjizade A, Ashrafzadeh SN, Sadeghi A (2017) Effect of ion partitioning on the electrostatics of soft particles with a volumetrically charged core. *Electrochem Commun* 84:19–23
27. Reshadi M, Saidi MH (2018) The role of ion partitioning in electrohydrodynamic characteristics of soft nanofluidics: inclusion of EDL overlap and steric effects. *Chem Eng Sci* 190:443–458
28. Maurya SK, Gopmandal PP, Bhattacharyya S, Ohshima H (2018) Ion partitioning effect on the electrophoresis of a soft particle with hydrophobic core. *Phys Rev E* 98(2):023103
29. Peralta M, Arcos J, Méndez F, Bautista O (2020) Mass transfer through a concentric-annulus microchannel driven by an oscillatory electroosmotic flow of a Maxwell fluid. *J Non-Newton Fluid Mech* 279:104281
30. Li X-X, Yin Z, Jian Y-J, Chang L, Su J, Liu Q-S (2012) Transient electro-osmotic flow of generalized Maxwell fluids through a microchannel. *J Non-Newton Fluid Mech* 187:43–47
31. Liu Y, Jian Y, Liu Q, Li F (2015) Alternating current magnetohydrodynamic electroosmotic flow of Maxwell fluids between two micro-parallel plates. *J Mol Liq* 211:784–791
32. López-García JJ, Horno J, Grosse C (2003) Suspended particles surrounded by an inhomogeneously charged permeable membrane. Solution of the Poisson–Boltzmann equation by means of the network method. *J Colloid Interface Sci* 268(2):371–379
33. Born M (1920) Volumen und hydrationswärme der ionen. *Z Phys* 1(1):45–48
34. Nightingale E Jr (1959) Phenomenological theory of ion solvation. Effective radii of hydrated ions. *J Phys Chem* 63(9):1381–1387
35. Probst RF, Sengun M, Tseng T-C (1994) Bimodal model of concentrated suspension viscosity for distributed particle sizes. *J Rheol* 38(4):811–829
36. Karniadakis G, Beskok A, Gad-el-Hak M (2002) Micro flows: fundamentals and simulation. *Appl Mech Rev* 55(4):76
37. Landau L, Lifshitz E (1963) *Electrodynamics of continuous media*, vol 8(2). Elsevier, Pergamon
38. Duval JF, van Leeuwen HP (2004) Electrokinetics of diffuse soft interfaces. 1. Limit of low Donnan potentials. *Langmuir* 20(23):10324–10336
39. Bird RB, Stewart WE (2006) *Transport phenomena*. Wiley, Hoboken
40. Yeh L-H, Zhang M, Hu N, Joo SW, Qian S, Hsu J-P (2012) Electrokinetic ion and fluid transport in nanopores functionalized by polyelectrolyte brushes. *Nanoscale* 4(16):5169–5177
41. Chatwin P (1975) On the longitudinal dispersion of passive contaminant in oscillatory flows in tubes. *J Fluid Mech* 71(3):513–527
42. Kurzweg UH (1988) Enhanced diffusional separation in liquids by sinusoidal oscillations. *Sep Sci Technol* 23(1–3):105–117
43. Kang Y, Yang C, Huang X (2002) Dynamic aspects of electroosmotic flow in a cylindrical microcapillary. *Int J Eng Sci* 40(20):2203–2221
44. Thomas AM (2003) Unusual effects of oscillating flows in an annulus on mass transfer and separation. *Adv Space Res* 32(2):279–285
45. Harris HG Jr, Goren SL (1967) Axial diffusion in a cylinder with pulsed flow. *Chem Eng Sci* 22(12):1571–1576
46. The Math Works I (2020) *The math works*, Inc. Matlab. version 2020a. Computer Software www.mathworks.com/
47. Bird RB, Armstrong RC, Hassager O (1987) *Dynamics of polymeric liquids*. Fluid mechanics, vol 1. Wiley, New York
48. Liu Q, Jian Y, Yang L (2011) Alternating current electroosmotic flow of the Jeffreys fluids through a slit microchannel. *Phys Fluids* 23(10):102001
49. Hsu H-P, Lee E (2012) Counterion condensation of a polyelectrolyte. *Electrochem Commun* 15(1):59–62